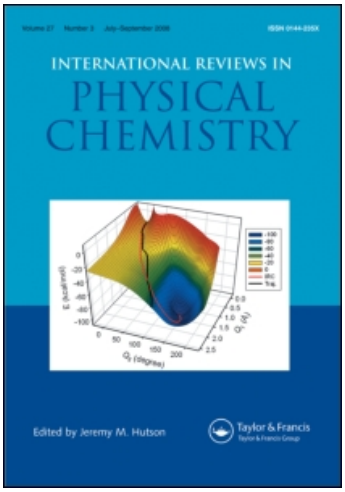

International Reviews in Physical Chemistry
Publication details, including instructions for authors and subscription information:
http://www.informaworld.com/smpp/title~content=t713724383

Amorphous and Poorly Crystalline Transition Metal Chalcogenides

R. R. Chianelli[a]
[a] Corporate Research Laboratories of Exxon Research and Engineering Co., Linden, NJ, USA

To cite this Article Chianelli, R. R.(1982) 'Amorphous and Poorly Crystalline Transition Metal Chalcogenides', International Reviews in Physical Chemistry, 2: 2, 127 — 165
To link to this Article: DOI: 10.1080/01442358209353332
URL: http://dx.doi.org/10.1080/01442358209353332

International Reviews in Physical Chemistry (1982), *2* (127–165)

AMORPHOUS AND POORLY CRYSTALLINE TRANSITION METAL CHALCOGENIDES*

R. R. CHIANELLI

Corporate Research Laboratories of Exxon Research and Engineering Co., Linden NJ 07036, USA

ABSTRACT

Crystalline transition metal chalcogenides have evoked considerable interest in the physics and chemistry community. The transition metal chalcogenides also exist in amorphous and poorly crystalline forms which have particularly useful catalytic and electrochemical properties. In this review we discuss the current understanding of the preparation, properties and structure of these compounds.

INTRODUCTION

The study of the chemistry and physics of solids has played an important role in many areas of great technological importance. The example of the semiconductor industry is perhaps the most striking, but many other examples are well known (electronic devices, optical devices, information storage devices, etc.) and many are under development, particularly in the areas of energy storage and energy conversion. These examples are based primarily on well crystallized materials and much of the basic understanding of these solids comes from studies on single crystals. However, future directions in solids research indicate an increasing emphasis on materials which are not well crystallized and contain various degrees of disorder. There are two reasons for this trend.

1. For large volume applications highly crystalline solids are often difficult and costly to manufacture (the recent emphasis on amorphous Si for photovoltaic devices applications is a good example).
2. Disorder is often inherent to successful application (high surface area heterogeneous catalysts are an example).

However, progress has been hampered because disordered solids are inherently more difficult to study because the lack of periodic order makes precise structural and electronic information unavailable. Such information can routinely be obtained when single crystals are available, but becomes increasingly difficult to obtain as the disorder increases. Structural information regarding disordered solids requires concerted application of diverse techniques. Recent developments in synchrotron X-ray techniques has added considerably to our arsenal of such techniques and, therefore, to

* Invited Paper presented at the Ninth International Conference on Amorphous and Liquid Semiconductors, Grenoble, France, 2–8 July 1981.

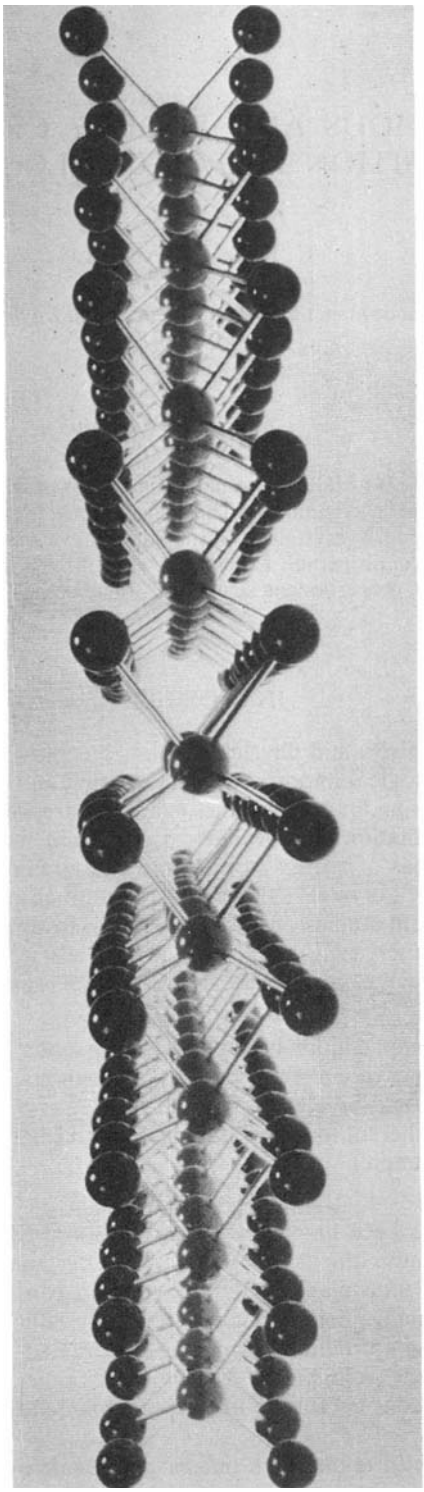

FIG. 1. The structure of MoS_2.

the solution of structural problems in disordered solids. Recent research on the class of compounds known as the amorphous and poorly crystalline transition metal sulfides specifically illustrates all of these features. Additionally, a third feature is illustrated; namely, introduction of disorder, as a degree of freedom in a class of crystalline compounds, greatly enhances the range of compositions, structures and properties available for study and application.

Major factors responsible for the current interest in crystalline transition metal chalcogenides are the highly anisotropic structures of these compounds and the wide variety of chemical and physical properties which these compounds exhibit. The anisotropy in these compounds can be illustrated by the structure of MoS_2 indicated in *Figure 1*. The structure can be viewed as a two-dimensional macromolecule. Each metal atom is bound to six sulfur atoms and each sulfur atom is bound to three metal atoms. Because the sulfur is so tightly bound its interaction with the next layer of sulfur above it is extremely weak. The only unsatisfied bonds are at the edge of the layer and these tend to be highly reactive as described further on. A similar situation exists for the transition metal trichalcogenides which have an anisotropic chain structure.

In this review the disordered transition metal chalcogenides which can be prepared in amorphous and poorly crystalline forms are described. In these forms the compounds exhibit all of the properties which their crystalline counterparts (if they exist) exhibit. Additionally, the amorphous analogs often exhibit interesting and useful properties which their crystalline counterparts do not. The preparation and the properties of these compounds are described. The structural problems associated with these compounds are particularly fascinating. The existence of highly anisotropic layers and chains in amorphous (to X-rays) compounds represents an interesting problem in the field of amorphous solids. The current understanding of the structure and the role of anisotropy in the chain-like trichalcogenides is described.

THE LAYERED TRANSITION METAL DICHALCOGENIDES

The layered transition metal dichalcogenides have found a wide variety of uses. Since before World War II, MoS_2 and WS_2 have been the basis for some of the most widely used hydrocarbon processing catalysts. (Weisser and Landa, 1973). MoS_2 has been used as a lubrication additive and TiS_2 as a cathode for lithium nonaqueous batteries (Whittingham, 1976). These applications arise in part from the highly anisotropic physical properties of these materials (Gamble *et al.*, 1970), which are due to their crystal structure. In this structure single layers of transition metals are sandwiched between two layers of close-packed chalcogen atoms. Within these layers the transition metal atoms are bound to six sulfur atoms which are arranged trigonal prismatically (MoS_2) or octahedrally (TiS_2) about the metal. Each sulfur atom bridges three transition metal atoms within the same layer, forming the only strong intralayer forces, and the layers can be viewed as two-dimensional macromolecules which stack, bound only by van der Waals forces, to form three-dimensional crystals (Schollhorn *et al.*, 1975). Because of this structural anisotropy the transition metal dichalcogenides tend to crystallize in basal plane dominated platey crystals like the one shown in *Figure 2*.

The transition metal sulfides which are known to crystallize in the layered structure are indicated in *Figure 3*. The wide variety of transition metals which exist in this structure coupled with the variability of the highly polarizable chalcogens (S, Se, Te) lead to a wide variation in the physics and chemistry of these solids. *Figure 4* schematically indicates simple band structures proposed for the layered dichalcogenides which can qualitatively account for their observed properties (Wilson and Yoffe, 1969).

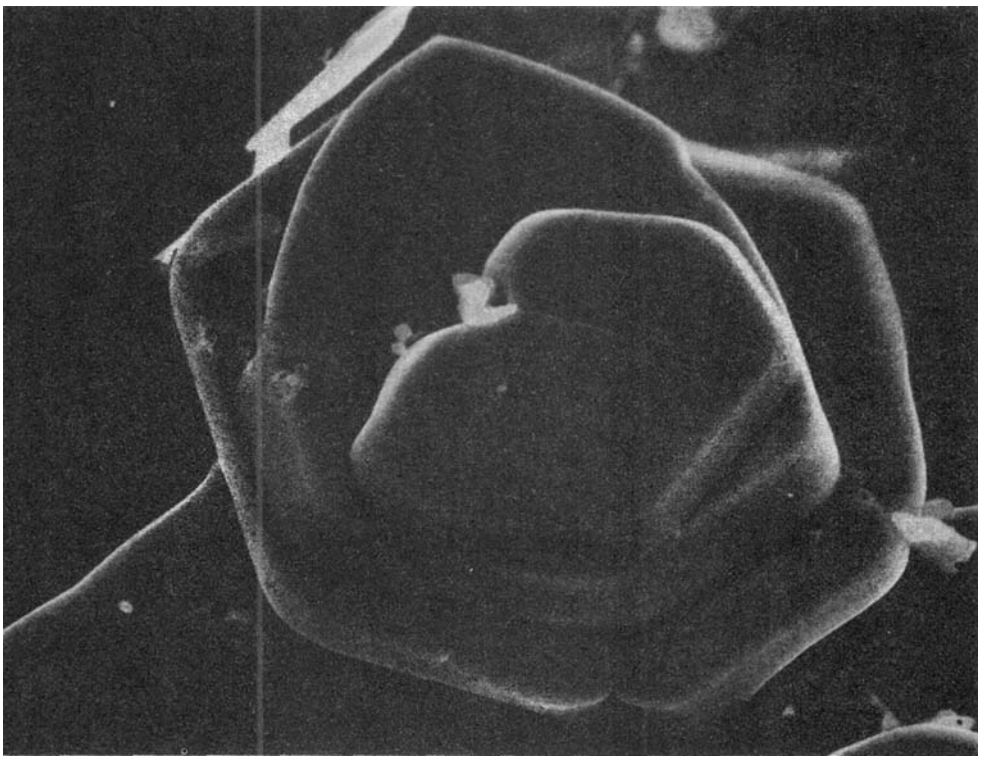

FIG. 2. Platey Habit of MoS_2(5 μ).

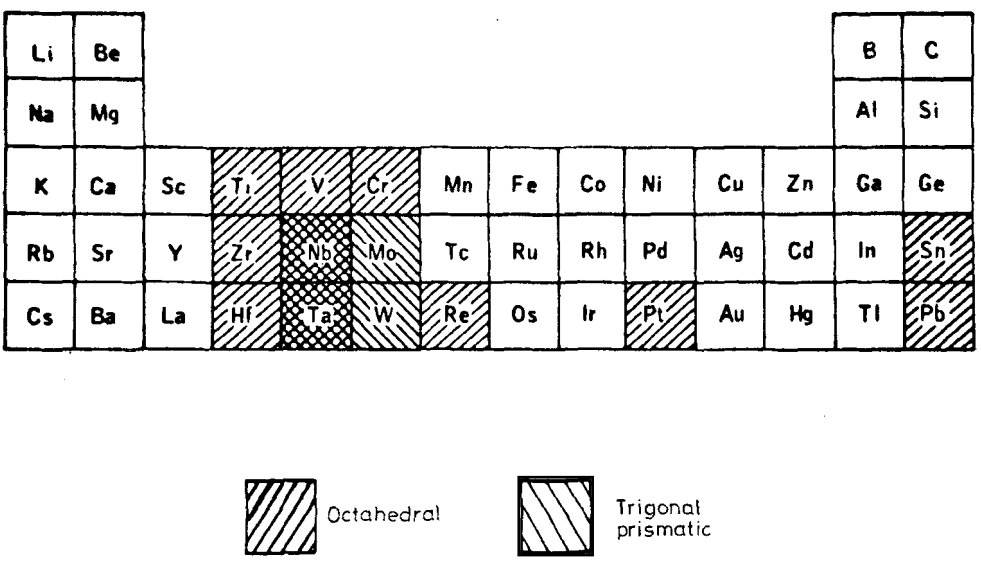

FIG. 3. The layered transition metal chalcogenides.

Group IV dichalcogenides which are octahedral are semiconductors with the exception of TiS_2 and $TiSe_2$ which are semimetals. In Group IV the valance band, consisting mostly of chalcogen s- and p-bonding orbitals, is filled, but the conduction band consisting mostly of metal d-character, is empty. In Group VI where the coordination is trigonal prismatic a narrow, two-electron band, which is filled, lies in the gap and the compounds are semiconducting. In Group V this band is half filled and the material is metallic. This simple picture is not sufficient of itself because the layered chalcogenides exhibit many interesting and often puzzling effects. The Group V dichalcogenides are superconducting (Gamble *et al.*, 1970) and several Group IV and V dichalcogenides have charge density wave transitions (Wilson *et al.*, 1969; Williams *et al.*, 1974). These effects are often enhanced by or have their origin in the anisotropic nature of these compounds.

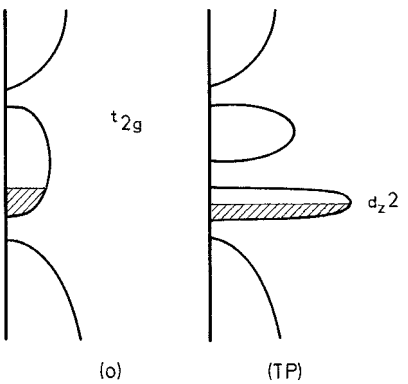

FIG. 4. Band structure of transition metal chalcogenides (reprinted with permission of the author, B. G. Silbernagel, *Materials Science and Engineering*, *31* (1977), 281).

The ability to insert (intercalate) alkali metals, organic bases and organometallic compounds between the layers of the transition metal chalcogenides is now a well known property of these compounds (Gamble, 1978). During this process the layers are separated from one another and an expansion of the lattice occurs which can in some instances be large, one of the largest (56 Å) being caused by the intercalation of octadecylamine in TaS_2 (*Figure 5*). The anisotropic macromolecular nature of the layers is clearly demonstrated in this case. Group IV and V dichalcogenides form most of the known intercalation compounds presumably because of their respectively empty and half filled conduction bands. Intercalation of a Group V dichalcogenide like NbS_2 with an alkali metal like lithium converts the metallic NbS_2 to the diamagnetic semiconducting $LiNbS_2$ because the conduction band is now filled. MoS_2 which has a filled conduction band forms very few intercalation compounds and those only with great difficulty.

Flexibility of the transition metal dichalcogenide layers

An example of disorder in the transition metal dichalcogenides is seen during the intercalation process itself. The ternary phase Li_xTiS_2 ($0 \leqslant \chi \leqslant 1$) has been the subject of intense study because of its superior performance as the active cathode material in a reversible lithium nonaqueous battery system (Thompson and Whittingham, 1977;

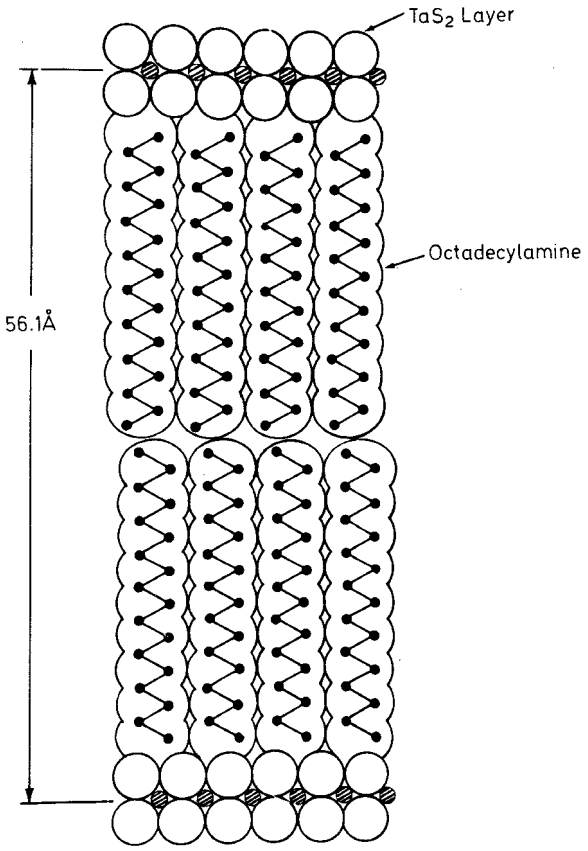

FIG. 5. The intercalation of octadecylamine in TaS_2 (reprinted with the permission of the author, F. R. Gamble, *Annals of the New York Academy of Sciences, 313* (1978), 86).

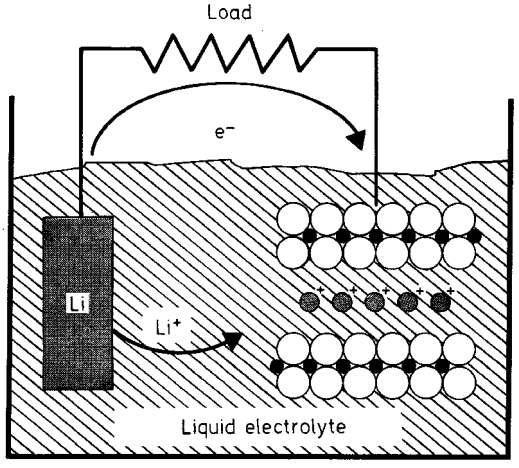

FIG. 6. Schematic of $LiTiS_2$ cell.

Whittingham, 1978). The reversibility of the TiS_2 cathodes arises in part from the unusual morphological nature of the intercalation reaction in which the lithium atoms slip into the van der Waals gap between the TiS_2 layers (*Figure 6*). This process occurs at the cathode during discharge from $\chi = 0$ (TiS_2 fully charged) until $\chi = 1$ ($LiTiS_2$ fully discharged) with intermediate values of x in Li_xTiS_2 occurring in between. Upon recharge the reverse process occurs with reformation of the fully charged TiS_2. During charge and discharge no chemical bonds are broken and the TiS_2 layers remain intact. This type of reaction, in which structural integrity is retained, has been termed a topochemical reaction (of which the intercalation reaction is a special case) and the importance of topochemistry in determining cathode reversibility has been discussed (Whittingham and Chianelli, 1977).

During this process the layers are severely flexed (*Figure 7*). In large crystals this flexing can lead to severe cracking and degradation of the crystals (Chianelli, 1976). In smaller crystals this process can be followed dynamically by optical microscopy or by X-ray diffraction (Chianelli *et al.*, 1979b). A chemical lithiation procedure described by Chianelli (1976) was used for the optical studies. Crystals with perfect hexagonal morphology (<0.1 mm) showed the effect indicated in *Figure 7*. A front beginning at the edge, moved through the crystal until it disappeared at the center 4 to 5 h later for an average crystal of about 50 μ. Crystals which showed this effect were not cracked after intercalation was complete. A lattice expansion of approximately 10% occurs upon intercalation with lithium, and the front shown in the hexagonal crystallite (*Figure 7*) is the boundary between the expanded and unexpanded lattice (also shown schematically in *Figure 8*). The front is quite sharp initially but becomes broader as the center of the crystal is reached. Generally, the boundary between the TiS_2 and $LiTiS_2$

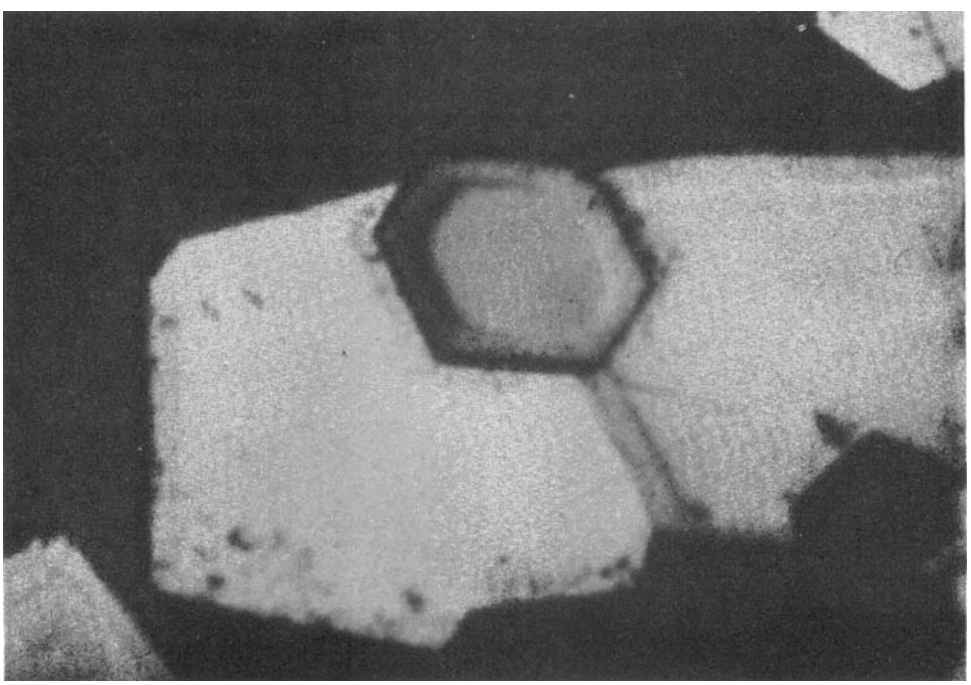

FIG. 7. Lithiation of perfect TiS_2 crystal (from Chianelli, 1976).

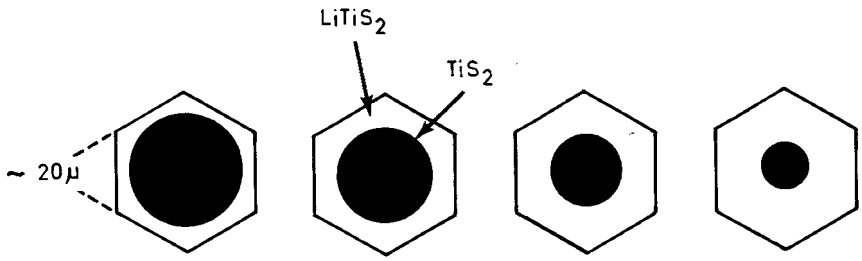

FIG. 8. Movement of front through TiS_2 crystal.

portions of the crystal was about 2 μ. X-ray studies of the η-butyllithation of TiS_2 with time showed the presence of 001 reflections of intercalated and unintercalated material with smearing between them, in agreement with the optical study.

The width of the transition zone was found to be $2 \pm 1\ \mu$ in all cases. Thus, large crystals (50 μ) appear to have fairly sharp boundary areas whereas smaller crystals (5.6 μ) have sloping less-well-defined fronts. The estimation of the boundary width depended to a certain degree on the observation techniques used and could not be determined to better than $\pm 1\ \mu$ for the larger crystals.

This dynamic layer bending leads to interesting effects in X-ray diffraction. We have previously described the construction of an X-ray cell which allowed monitoring of structural changes at the TiS_2 cathode (or anode) during electrochemical operation (Chianelli *et al.*, 1979b). *Figure 9* shows schematically the construction of the cell which allows X-rays to probe the cathode through a beryllium window, while simultaneously monitoring the electrochemical potential of the cell via external leads (for details *see* Chianelli *et al.*, 1979b). This technique allows continuous monitoring of the Bragg reflections as a function of x in the non-stoichiometric compound Li_xTiS_2 for $0 \leqslant x \leqslant 1$. *Figure 10* shows a complete curve for this range determined by following the 101 Bragg peak. The plateau in the curve was later shown to be due to lithium ordering in two dimensions between the layers (Thompson, 1978).

Throughout the experiments, the width of the 101 line for a given x in Li_xTiS_2 did not change, but the intensity of the peak decreased. This decrease cannot be explained by calculating the intensity of the 101 line for various compositions of Li_xTiS_2. Because of the low scattering power of lithium atoms, no more than 10% variations is expected in the intensity of the 101 line, whereas a decrease of more than 50% is observed, as seen in *Figure 10*. Experiments indicated that upon standing on open circuit for 10 h, this

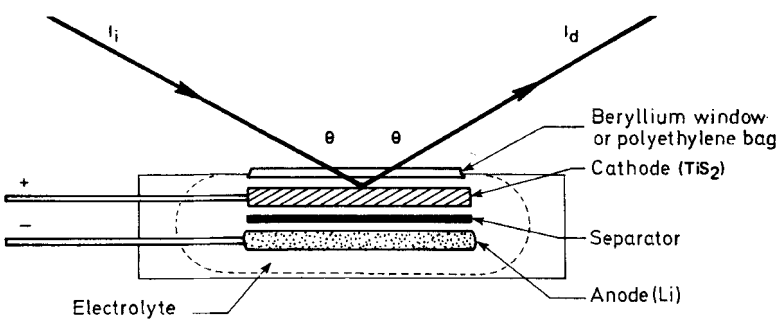

FIG. 9. Dynamic X-ray diffraction cell (from Chianelli *et al.*, 1979b).

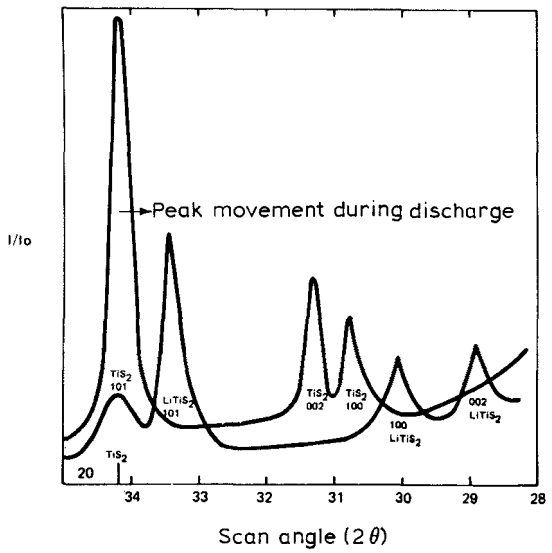

FIG. 10. Movement of Bragg peaks during lithiation of TiS_2 (from Chianelli *et al.*, 1979b).

intensity is regained almost to the original value. We believe that the observed intensity loss (to diffuse scattering which is not easily observable using current cell design) during the discharge is due to intercalated layers which are wrinkled or bent, and therefore do not contribute to the intensity of Bragg peaks. Upon standing on open circuit, the stressed TiS_2 layers anneal and realign themselves, causing the intensity to be regained. This is in agreement with the previously described optical studies in which the crystals are highly strained during intercalation, then relax upon completion of reaction. In fact, it is probably the ability of the TiS_2 layers to flex and reorder which allows the TiS_2 to function so well as a secondary battery cathode. The above demonstrates the remarkable flexibility and macromolecular nature of these layers at the 1 μ level. We believe that further work in this area would lead to a description of the kinetic processes of intercalation in terms of the fundamental mechanical properties of the layers which can further be described by atomic bonding properties.

Low temperature preparation of transition metal dichalcogenides

All of the interesting properties described above have been observed in crystalline compounds. Conventionally these compounds have been prepared only by high temperature (above 400°C) methods such as direct contact of the elements in sealed tubes or vapor-phase reaction of the halides with hydrogen sulfide (Thompson *et al.*, 1975). The elevated temperatures are necessary to obtain reasonable rates of reaction and/or favorable thermodynamics. The products thus obtained are typically highly crystalline, are of low surface area, and are often non-stoichiometric and multiphased unless extensive care is taken during preparation. Recently a general method of preparing the transition metal dichalcogenides at or near ambient temperatures has been reported (Chianelli and Dines, 1978). The materials thus produced have physical properties radically different from those produced at higher temperatures. By

appropriate adjustment of parameters, poorly crystalline or amorphous powders, gels, glasses, or homogeneous dispersions of chalcogenides can be prepared. Additionally, normally crystalline compounds can be prepared, and because the preparations take place below 400°C, portions of the transition metal-sulfur phase diagrams not previously studied are accessible (VS_2, for example).

Low temperature metathetical reactions in solution (Eq. (1)),

$$TX_4 + 2A_2Y \xrightarrow{\text{soln}} TY_2 + 4AX \tag{1}$$

where T = transition metal; X = salt anion (Cl^-, carboxylate, etc.); A = alkali-like cation (Li^+, Na^+, NH_4^+, etc.); and Y = chalcogenide anion, present an attractive alternative means of preparation since they should be fast, simple, and allow for some control over parameters such as particle size and composition. Since both the transition-metal ions and chalcogenides are capable of existing in several oxidation states, redox reactions such as Eq. (2) can also be conceived:

$$TX_5 + \tfrac{5}{2}A_2Y \xrightarrow{\text{soln}} TY_2\downarrow + 5AX + \tfrac{1}{2}Y \tag{2}$$

The high stability of the oxides and hydroxide of the early transition metals rules out aqueous environments for all such reactions; in fact, hydroxylic solvents in general (alcohols and carboxylic acids) are too reactive to serve as solvents for TX_4 or TX_5. Furthermore, hydrogen sulfide is not a viable source of chalcogenide ion at ambient temperature, since only traces of product form with $TiCl_4$, whether it is neat or is dissolved in a polar organic solvent.

We may illustrate the technique by considering TiS_2. Even in the absence of oxygen from air to water, the reaction of $TiCl_4$ with H_2S has an unfavorable equilibrium direction at temperatures less than about 400°C:

$$TiCl_4 + 2H_2S \xrightarrow{400°C} TiS_2 + 4HCl \tag{3}$$

By using a more reactive (ionic) source for the chalcogenide (or equivalently by 'activating' hydrogen sulfide by the addition of ammonia or amines) the reaction to form the transition-metal chalcogenides proceeds readily and quantitatively at ambient temperatures. Lithium sulfide was found to be the most convenient source of sulfide ion:

$$TiCl_4 + 2Li_2S \xrightarrow{25°C-100°C} TiS_2 + 4LiCl \tag{4}$$

Convenient solvents for ambient-temperature precipitation were tetrahydrofuran (THF) or ethyl acetate (EA). Both afforded dark precipitates which were easily filtered. The TiS_2 produced was amorphous to X-rays but in other aspects such as reaction with η-butyllithium behaved as normal crystalline TiS_2 as described below. It proved difficult, however, to completely remove the LiCl because of the tenacious affinity of the highly active sulfide either on their surfaces or as inclusion compounds. However, repeated washings with the solvent would completely remove the LiCl. Crystalline TiS_2 powders could be produced by heating amorphous TiS_2 at 400–600°C in sealed quartz tubes with careful exclusion of oxygen. Crystalline TiS_2 could be produced in the same temperature range as the amorphous TiS_2 by letting the reaction proceed much more slowly.

Single crystals of TiS_2 up to 100 μ in diameter were grown from refluxing THF (tetrahydrofuran) in a Soxhlet extractor. Li_2S was placed in the extraction thimble and was slowly leached by refluxing THF. This occurred quite slowly, and after about 2 weeks approximately 100 mg of golden crystals of TiS_2 was isolated from the flask. These crystals were well formed and ranged in size from 50 to 150 μ. This experiment clearly demonstrates that crystalline TiS_2 can be prepared from $TiCl_4$ and Li_2S at temperatures as low as 65°C. This result indicates that the amorphous TiS_2 is either a metastable phase or consists of randomly folded sheets of TiS_2 which have not been allowed to crystallize by the rapidity of precipitation.

During the study of nonaqueous precipitation it was discovered that under various conditions (described in Eq. (5)) gels could be produced. These gels, if pumped and heated to greater than 300°C, yielded a black, glassy solid having an amorphous X-ray powder diffraction pattern. Scanning electron microscopy (SEM) revealed conchoidal fracture surfaces indicating that the product was a glassy phase, and X-ray fluorescence analysis showed titanium and sulfur. However, this glass was very air sensitive and when heated in air would spontaneously ignite and yield a new glassy substance which showed broad TiO_2 diffraction lines. We may summarize the results as follows:

$$\underset{\text{R = hexyl}}{TiCl_4 + 4NR_3 + 2H_2S} \xrightarrow{\text{THF}} \underset{\text{gel}}{TiS_2 + 4R_3NHCl} \tag{5}$$

The fact that the gel does not form when NH_3 is used instead of the long-chain amine suggests that the size of the R group is critical to gel formation. Probably the long-chain amines which would be complexed to the newly formed TiS_2 stabilized gel formation. The gel then decomposes as follows:

$$TiS_2 \text{ gel} \xrightarrow[-\text{THF}\ -\text{HCl}\ -\text{RN}]{300^\circ\text{C}} TiS_2 \text{ glass} \xrightarrow{400^\circ\text{C}} TiS_2 \text{ crystalline} \tag{6}$$

$$TiS_2 \text{ glass} \xrightarrow[O_2]{400^\circ\text{C}} TiO_2 \text{ (poorly crystalline)}$$

During the course of studying the room-temperature precipitation of the layered sulfides it became apparent that under a wide variety of conditions the precipitated solid remained completely or partially dispersed. For example, when a yellowish solution of $TiCl_4$ in PC (propylene carbonate) was added to a white slurry of Li_2S in PC, the solution immediately turned intensely black. No solids could be filtered out and this liquid remained stable for several years. Since it was established in several ways that the reaction of $TiCl_4$ with Li_2S is a straightforward one yielding TiS_2 + LiCl, we recognize that this black liquid was likely a colloidal dispersion of TiS_2 in the dense liquid PC. Evidence points to a colloidal dispersion of the sulfur–metal–sulfur layers. Indeed, Murphy and Hull (1977) and Serf and Schollhorn (1977) have reported the preparation of aqueous dispersions of TaS_2 produced by electrochemical exfoliation and dispersion by blending with a surfactant. During this process hydrogen is electrochemically intercalated in the TaS_2 as protons forming H_xTaS_2. Upon relaxing the circuit the protons spontaneously recombine to form hydrogen molecules. The resulting rapidity of the reaction and expansion of the lattice literally causes the crystal to explode into the solvent. The surfactant in the water helps stabilize the dispersion of layers. All of this is not too surprising in view of the previously described huge lattice expansion which occurs when steramide, itself a surfactant intercalates in TaS_2.

These dispersions were black with platelets in the 0.25–2 μ range but were unstable to hydrolysis by the aqueous solution. The dispersions made by the low temperature

techniques are more stable and often show a twinkling effect under high-power microscope objectives, but the particles giving rise to this effect are unresolved indicating that they are below 1 μ in size. The dispersions are optically very black, and no other detail above the general scattering background could been seen in visible-light transmission spectrographs which are shown in *Figure 11* for a MoS_2 dispersion. The two small bumps which can be seen just above the background are due to starting $MoCl_4$ and they can completely be removed by allowing more reaction time.

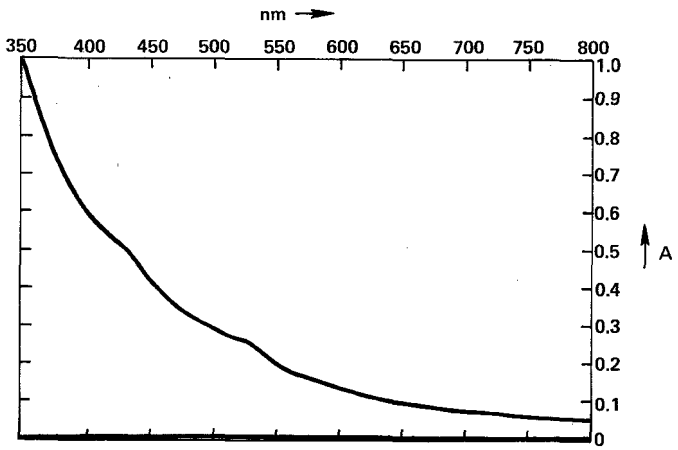

FIG. 11. Optical adsorption spectrum of MoS_2 dispersion (from Chianelli and Dines, 1978).

Propylene carbonate was the most effective dispersing solvent tried with the concentration of TiS_2 reaching 0.2 M before the solid began to separate. Other solvents were also able to disperse the layered sulfides to a greater or lesser extent. Generally, polar solvents with high viscosity and boiling points were the best dispersants. Dimethylformamide yielded wine-colored, purple, or dark blue dispersions depending upon the concentration which was generally lower than that obtained in propylene carbonate. Addition of amines such as pyridine increased the ability of a particular solvent to disperse. The dispersed sulfides could be adsorbed from solution on basic oxides such as MgO or CaO because of the Lewis acid nature of the layered transition-metal sulfides or the nature of the polar adlayer. Adding sufficient basic oxide can entirely clear a solution. The amount of sulfide adsorbed (for a given stirring rate and particle size) depended upon the contact time with the dispersion and the concentration for a given basic oxide.

TABLE 1. η-Butyllithium uptake

Sample	*Uptake* (mol)
TiS_2	1.09
VS_2	1.48
MoS_2	1.51

The amorphous sulfides reacted with a solution of η-butyllithium in hexane in a similar manner to that reported for the crystalline layered sulfides (Murphy *et al.*, 1975). The amount of lithium taken for three samples is indicated in *Table 1*.

The reaction which causes the crystalline dichalcogenides to intercalate lithium has often been used as a 'test' for the purity of the crystalline materials. In this respect amorphous TiS_2 behaves just like crystalline TiS_2 giving further evidence that its structure is similar to TiS_2. The same statement can be made for amorphous VS_2 which cannot be made crystalline except by deintercalating the crystalline compound $LiVS_2$ (Murphy *et al.*, 1975) which can then be intercalated. However, as previously stated crystalline MoS_2 does not intercalate lithium and the fact that the amorphous material does indicates that the structure is probably different to that of the crystalline material. Also as we shall see later, this is an example of a useful and interesting property exhibited by the amorphous sulfide which its crystalline analog does not exhibit. Work continues on these preparative techniques, but we can see that a class of materials whose crystalline counterparts exhibit many interesting and useful properties can now be prepared in a variety of new forms which themselves exhibit interesting and potentially useful properties. At the moment we know most about the properties and structure of the partially crystallized (poorly crystalline) and amorphous dichalcogenides. The remainder of this section will be devoted to these two classes of materials.

Disordered layers—poorly crystalline dichalcogenides

The poorly crystalline dichalcogenides are prepared by heating in a sulfiding atmosphere the amorphous dichalcogenides prepared by the methods described in the previous section. This heating causes the dichalcogenides to crystallize partially in a structure which we have termed the 'rag' structure (Chianelli *et al.*, 1979a). For example, we prepared the material shown in *Figure 12* by heating several grams of amorphous MoS_2 for 2 h at 400°C in a stream of H_2 mixed with 15% H_2S. The rag depicted in *Figure 12* consists of several stacked but highly folded and disordered MoS_2 layers. Although only 20 to 30 Å thick in the stack direction, the layers extend several thousand angstroms perpendicular to the stack direction. By varying the conditions of preparation, one can vary the number of stacks and the dimensions of the layers. Above we described the flexibility of the layers in TiS_2 as exhibited during the intercalation of lithium into single crystals. The existence of the rag structure further demonstrates the flexibility and macromolecular nature of the dichalcogenide layers, but the layers now occur in a more highly disordered form. *Figure 13* illustrates a typical scan that is characteristic of poorly crystalline layered disulfides; it is similar to the scan reported by Wildervanck and Jellinek for MoS_3 (Wildervanck and Jellinek, 1971). It exhibits a strong 002 maximum in the low-angle region and a broad envelope beginning approximately at $2\theta = 30°$ and continuing out to above $2\theta = 60°$. This envelope contains the 100, 101, 102, 103, 006, 105, 106, 110, and 008 reflections with well-defined maxima appearing for the 100, 103, and 110 reflections. The maximum at 103 indicates that the 2H (two layer hexagonal) molybdenite stacking sequence is retained in some crystallites. The asymmetric shape of the 100 envelope is characteristic of random layer lattice structures (Guinier, 1963), in which the layers are displaced randomly with respect to one another like a spread deck of cards. They are stacked normally, although the position of the 002 reflection is displaced slightly to lower angles; this displacement is presumably due to imperfect stacking, as has been described for graphite (Ergun, 1968). When a mixed reflection such as the 103 reflection appears, its line width indicates that the two-layer molybdenite stacking sequence is maintained for at least two stacks, as might be expected. We also observed that pressing the 'poorly crystalline' MoS_2 in a laboratory press at approximately 100 atm significantly increased the sharpness of the X-ray reflections, presumably improving the stacking of the rags. There is considerable non-Bragg scattering present at low angles. This may be due to

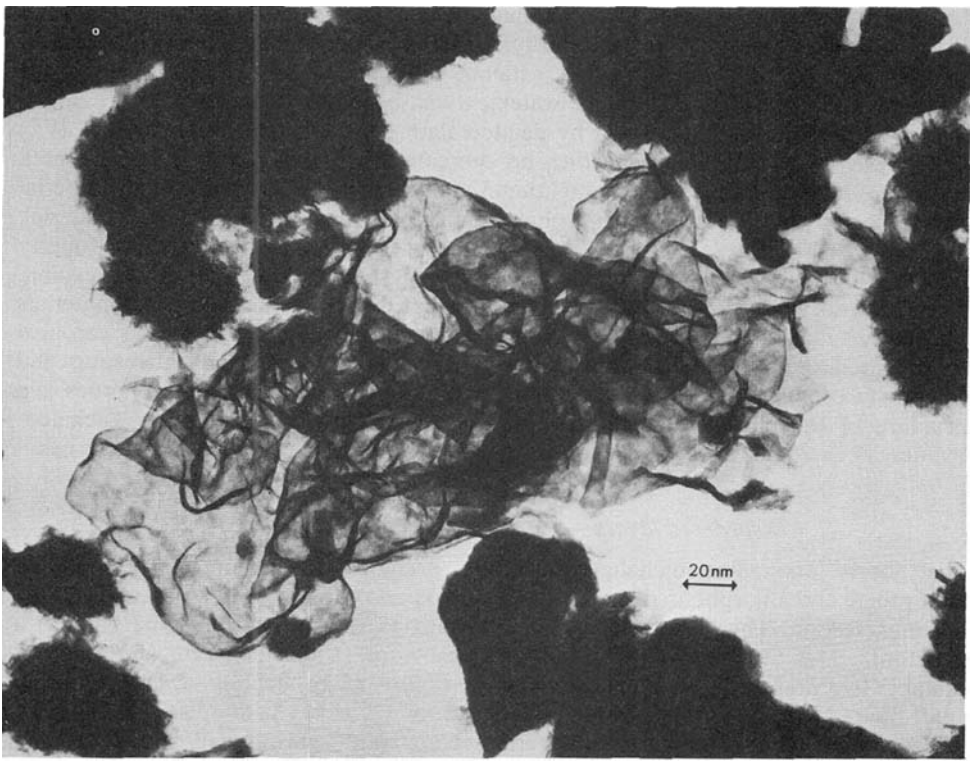

FIG. 12. MoS_2 in the 'rag' structure.

uncorrelated single layers and the pore structure that they generate by randomly folding and connecting with other sheets. All of the above observations are consistent with the stacking and folding of individual MoS_2 layers to form a highly disordered, poorly crystalline MoS_2.

WS_2, ReS_2, and OsS_2 can also be prepared in the poorly crystalline form by heating the amorphous sulfides in a H_2/H_2S atmosphere at 400°C (Pecoraro and Chianelli,

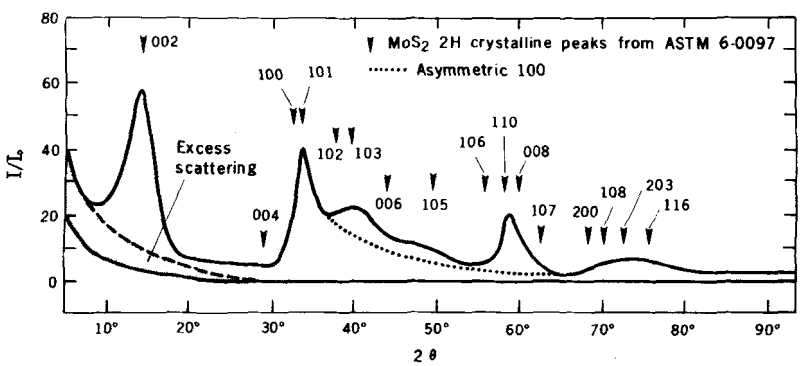

FIG. 13. Diffraction from poorly crystalline MoS_2 (from Chianelli *et al.*, 1979a).

TABLE 2. Indexing of layered diffraction patterns

		MoS_2		WS_2	
	hkl	*d*	*I/Io*	*d*	*I/o*
00ℓ	002	6.15	100	6.18	100
	004	3.08	4	3.09	14
	006	2.049	14	2.061	12
	008	1.538	12	1.546	8
hk0	100	2.737	16	2.731	25
	110	1.581	12	1.578	16
h0ℓ	101	2.674	10	2.667	25
	102	2.501	8	2.498	8
	103	2.277	45	2.277	35
	105	1.830	25	1.836	18
	106	1.641	4	1.646	

1981). The X-ray diffraction patterns for ReS_2, OsS_2, and MoS_2 are compared in *Figure 14*. All exhibit a strong maxima in the low angle region, which corresponds to the 002 Bragg reflection in the ideal hexagonal layered structure and a broad envelope beginning approximately at 30° (2θ) and continuing out to above 60° (2θ). For MoS_2 and WS_2 all of the expected Bragg peaks can be identified as indicated in *Table 2*. This is

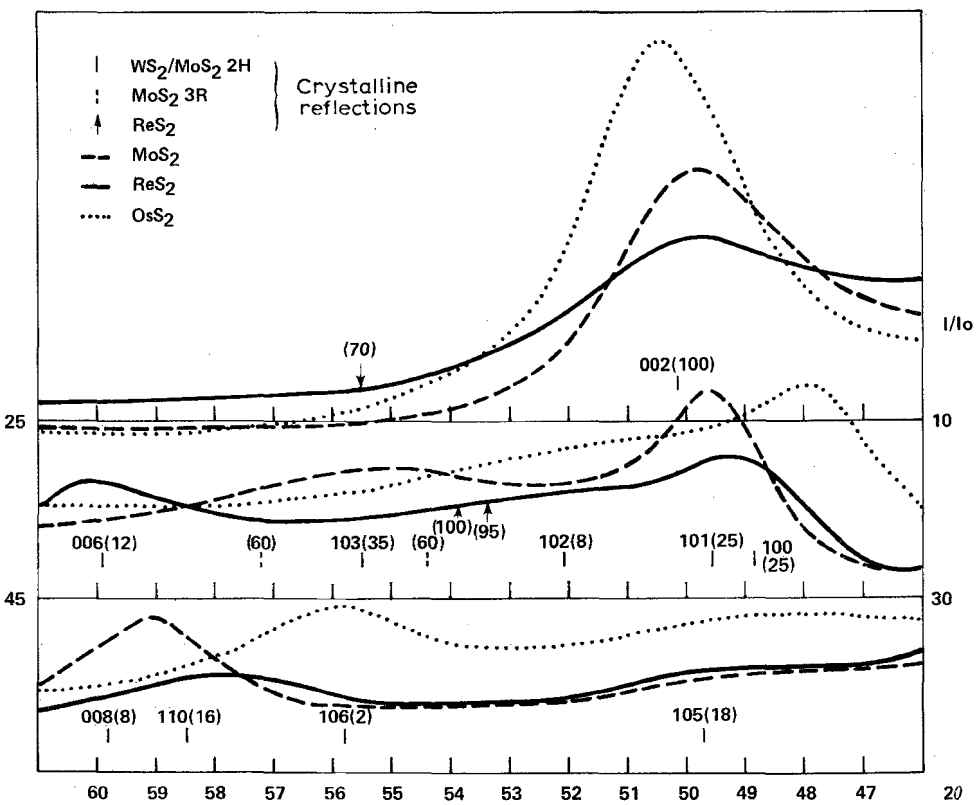

FIG. 14. Poorly crystalline X-ray patterns of the layered sulfides.

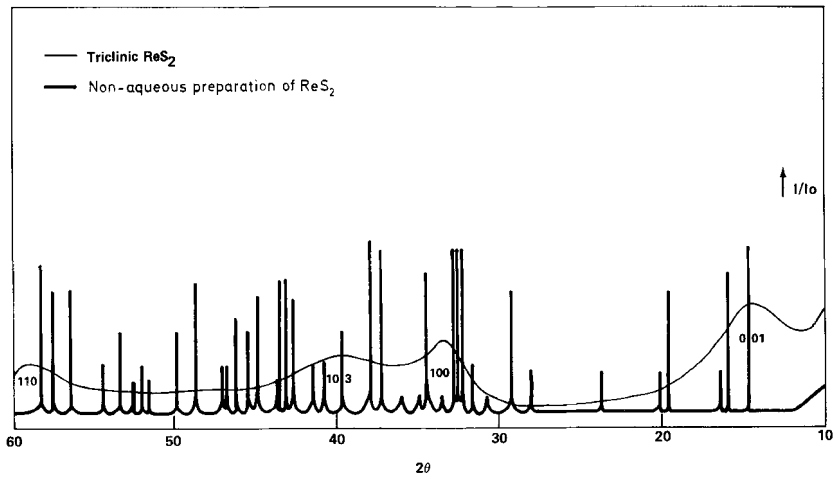

FIG. 15. Poorly crystalline ReS_2 (from Pecoraro and Chianelli, 1981).

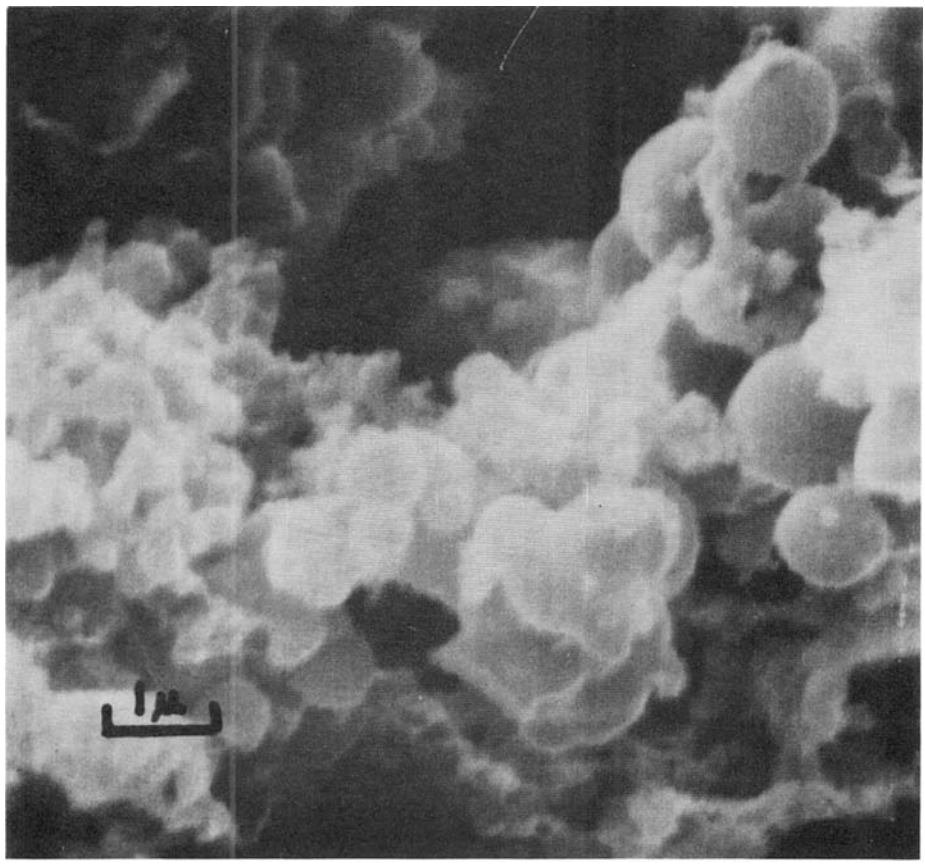

FIG. 16. ReS_2 spheres (1 cm = 1 μ) (from Pecoraro and Chianelli, 1981).

not the case for ReS_2 (*Figure 15*) which in its crystalline form is triclinic due to metal bonding which distorts the lattice (Alcock and Kjeckshus, 1965). At this time the structural difference between poorly crystalline ReS_2 and crystalline ReS_2 is unresolved. However, it appears that the poorly crystalline ReS_2 has the 2H structure and we do not know if it contains the metal–metal bonds which lead to the triclinic distortion in crystalline ReS_2. ReS_2 prepared from $ReCl_5$ often shows the unusual morphology indicated in *Figure 16*. The SEM micrograph reveals many perfect spheres in the 0.1–1.0 μ range. A rough calculation shows that the surface area of spheres would be about 10 m^2/g agreeing with the measured surface areas. However, X-ray line broadening analysis indicates crystallite size of about 74 Å perpendicular to the c-axis and 35 Å parallel to the c-axis, giving a calculated surface area of 95 m^2/g.

A possible model of the structure of these spheres is indicated in *Figure 17*. This model is similar to the 'fringed micelle' concept familiar to polymer chemists and further demonstrates the macromolecular nature of the layered sulfides. This behaviour is reminiscent of layered $TiCl_3$ propylene polymerization catalysts which also show spherical structures after extensive ball milling. During the ball milling the surface area of the $TiCl_3$ at first increases but then drops as the layers aggregate forming spherical structures (Tornqvist *et al.*, 1967).

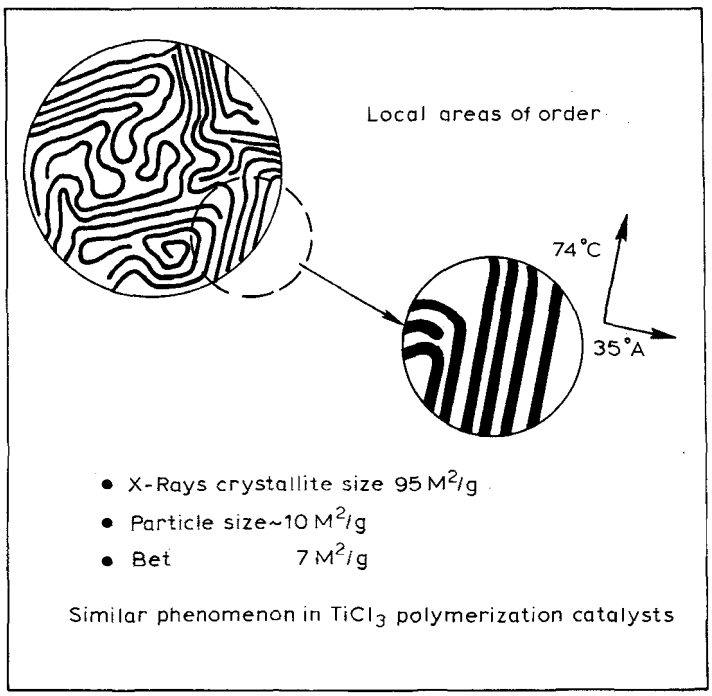

FIG. 17. 'Fringed micelle' model of ReS_2.

ReS_2 in the poorly crystalline form exhibits the most extreme morphological effects of the disordered layer lattice structure. The model for poorly crystalline ReS_2 embodies all three elements for these materials which we have so far discussed.

1. Retention of the local order found in the crystalline analogs.
2. Random folding of layers on a 50–150 Å scale.
3. Aggregation of randomly folded layers in spheres on a scale of greater than 500 Å.

Diffraction modeling of MoS_2

The above description of the structure of poorly crystalline MoS_2 is based primarily upon morphological evidence derived from electron microscopy and qualitative analysis of X-ray diffraction. The X-ray diffraction patterns contain a considerable diffuse component. Limited structural information, mainly on the crystallite size, may be determined using X-ray line broadening analysis on the 002, 100 and 110 peaks. However, the diffuse nature of the 103, 105 and other higher order peaks cannot be simply explained. In fact, comparison of the diffraction patterns of poorly crystalline MoS_2 with that of crystalline MoS_2 reveals other features such as shifting of the peak positions and asymmetric broadening of the peaks. Most Bragg peaks in this case are not amenable to detailed line profile analysis (*Figure 13*) and a strong diffuse background is present in the 100–103–105 region (as marked by the dotted line). However, quantitative information may be obtained by directly computing the diffraction pattern from an assumed structure using the Debye Scattering equation as described in a recent publication (Chien *et al.*, 1981):

$$I_{eu} = \sum_m \sum_n f_m f_n \frac{\sin |S| r_{mn}}{|S| r_{mn}} \tag{7}$$

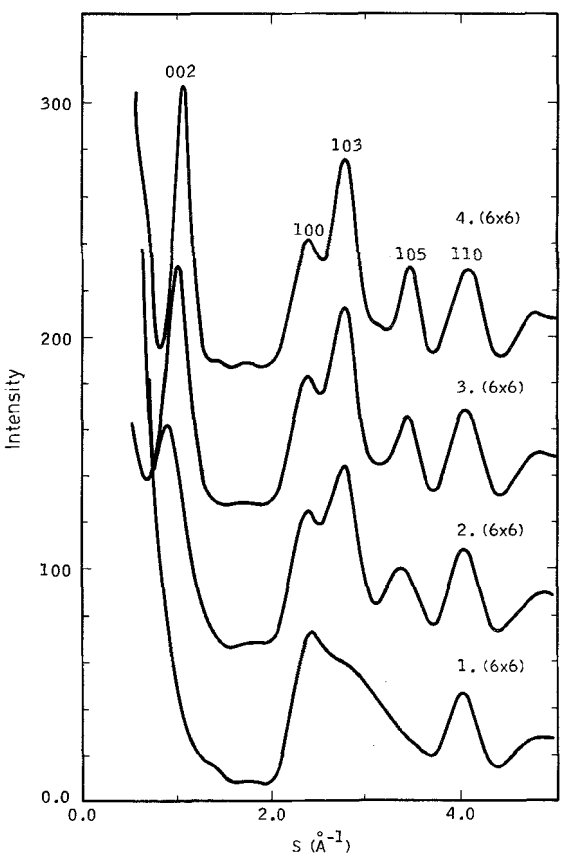

FIG. 18. Calculated X-ray diffraction of small (6 × 6 Mo atoms) crystallites of MoS_2 with 1–4 stacked layer (from Chien *et al.*, 1981).

Where f_m is the X-ray atomic scattering factor of m-type atoms, S is the X-ray scattering vector with $|S| = 4\pi \sin \theta/\lambda$, and the vector r_{mn} is the distance vector connecting atom m and atom n. For a structure in which all of the atomic positions have been specified, the diffraction intensity is directly calculated using Eq. (7).

We can see from *Figure 18* that all of the essential features of the diffraction pattern *except* the 002 peak are contained in the calculated pattern of a single (6 × 6) layer. The 002 peak is due to subsequent stacking of layers as indicated in *Figure 18*. However, ordered stacking introduces too much detail in the diffraction pattern. In fact, for a

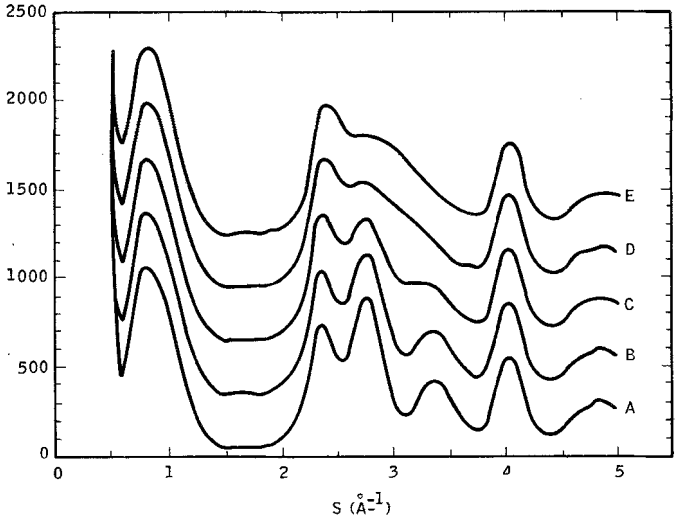

FIG. 19. The effect of interlayer rotation about the c-axis (A = 0.0, E = 0.1 radian) (from Chien *et al.*, 1981).

particular poorly crystalline diffraction pattern (similar to *Figure 13*) no reasonable fit could be obtained with a microcrystallite model. Thus, an imperfect crystallite model is required to fit satisfactorily the diffraction data. As previously indicated the MoS_2 layers appear to be highly flexible. However, introducing a modest bending of the layers produces only a small effect in the interference function and cannot account for the observed diffraction patterns. However, rotation about the c-axis leaves 002 unchanged and quickly brings the rest of the pattern into agreement with the experiment. *Figure 19* shows the diffraction patterns of a two layer stack with each layer containing 64 molybdenum atoms (2 · (8 × 8)) structure with the two sandwich layers rotated about the c-axis with respect to each other through an angle of 0.0, 0.02, 0.04, 0.08 and 0.1 radian, respectively. These structural changes have little effect on the 002 and 110 peaks. However, the effect on the 100–103–105 region is quite close to that of the single layer structure shown in *Figure 18*. The degree of this interlayer rotation can therefore be one of the most important structural parameters in the determination of the diffuse X-ray diffraction pattern of poorly crystalline MoS_2. Combining this simple disorder parameter with the other 2 parameters N and L (N = number of Mo and L = number of stacks) should, in principle permit a good quantitative fit to the various stages poorly crystalline MoS_2. In *Figure 20*, a comparison is shown of the calculated and experimental results using a diffraction pattern of MoS_2 prepared at 400°C. In *Figure 20*, the raw data is used in the plot without such corrections as Compton scattering, polarization, and absorption, and it is not properly scaled. These corrections ultimately are

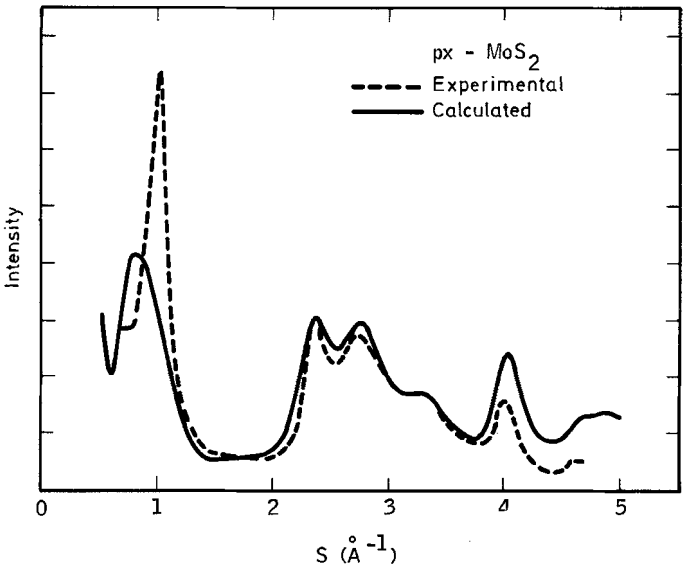

FIG. 20. Comparison of the measured and calculated X-ray scattered intensity for poorly crystalline MoS_2 (from Chien *et al.*, 1981).

needed in order to yield the coherent part of the scattered intensity for a direct comparison with the calculation. On the same figure a calculated curve (*Figure 19D*) is chosen for comparison and the two are arbitrarily set equal at $S = 2.3$ Å^{-1}. The fit is very good except at $S - 1$ Å^{-1} (002). This presents no problem as the number of layers increases, the 002 peak is sharpened and shifted to higher $|S|$ without seriously altering the rest of the pattern. It is clear from *Figure 20*, both at 002 and for the 100–103 splitting, that we require closer to 4 layers than the 2 used here. The fall off at larger $|S|$ ($S = 4 \sim ^{-1}$) can be largely attributed to the need for a polarization and absorption correction.

Catalytic importance of poorly crystalline layered dichalcogenides

Knowledge of the disorder in poorly crystalline MoS_2, WS_2 and ReS_2 becomes important when considering the catalytic properties of these solids. MoS_2 and WS_2 have been the industry 'work horses' for removal of sulfur from petroleum feedstocks prior to further refining (Weisser and Landa, 1973). Usually they are used in conjunction with a 'supporting' material such as Al_2O_3. In spite of their industrial importance the fundamental basis for their catalytic activity is poorly understood. Unsupported poorly crystalline MoS_2 exhibits catalytic activity in model and real hydrodesulfurization (HDS) reactions. Normally, one attempts to relate catalytic activity to simple N_2 adsorption (BET) surface area measurements. The poorly crystalline MoS_2 previously described have surface areas which fall into the 25–100 m^2/g region. Since X-ray line broadening measurements on poorly crystalline MoS_2 do not reflect actual particle sizes, knowledge of the disordered rag structure of poorly crystalline MoS_2 helps in understanding the surface area measurements. In fact, one can obtain some agreement between measured and calculated surface areas by assuming that the sheets are infinite in extent and the surface area is dependent only upon the extent of crystallite stacking. Stack numbers obtained from surface area measurements and from 002 line broadening measurements are then in reasonable agreement (Chianelli *et al.*, 1979a).

Further, HDS catalytic activity measurements *do not* generally correlate to N_2 BET

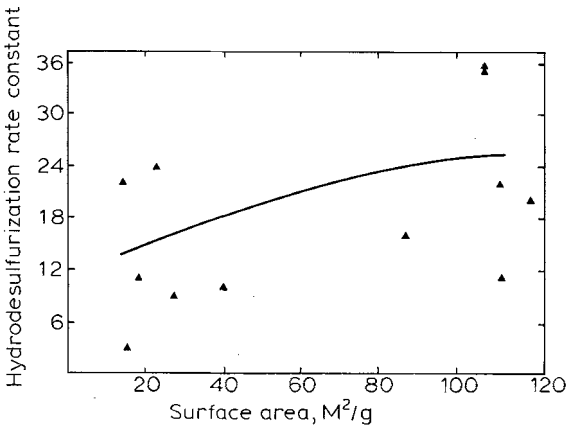

FIG. 21. Hydrodesulfurization activity vs. surface area for MoS_2 (from Tauster *et al.*, 1980).

surface area measurements as indicated in *Figure 21*. They do, however, correlate to a specific chemisorption technique in this case O_2 chemisorption (*Figure 22*). It is believed that this result arises from the anisotropy of the layered structure. The basal planes of the catalyst are extremely inert contributing to the N_2 surface area measurement but not to the catalytic activity. O_2 on the other hand chemisorbs on the MoS_2 edge planes where the catalytically active sites are located (Tauster *et al.*, 1980). Again this emphasize the macromolecular nature of these sheets. Flexible, inert basal planes dominate the intercalation chemistry and disorder in the layered chalcogenides. But, chemically active terminating planes dominate the catalytic properties of the layered chalcogenides. In a disordered material such as that shown in *Figure 12* the situation is more complex where well defined crystallographic edges do not appear but obvious defects do appear. It can be seen that a thorough knowledge of the nature of disorder and defects in these materials will greatly enhance our understanding of the basis for and improvement of catalytic activity.

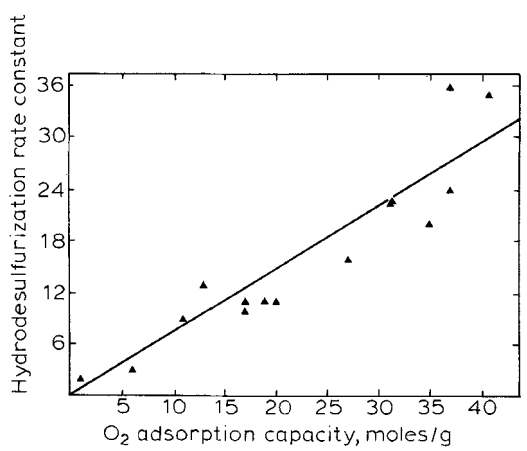

FIG. 22. Hydrodesulfurization activity vs. O_2 chemisorption for MoS_2 (from Tauster *et al.*, 1980).

Amorphous dichalcogenides

A previous section described the preparation of the transition metal dichalcogenides by low temperature precipitation from non-aqueous solvents. In the appropriate solvent a solid amorphous dichalcogenide can be isolated having a sulfur to metal ratio near 2. *Table 1* indicates one property of the amorphous dichalcogenides (uptake of lithium) which indicates that the behavior of the amorphous solids can be significantly different to that of their crystalline counterparts. In the following section the amorphous dichalcogenides will be examined in greater detail.

Amorphous MoS_2 can be prepared as previously described by adding with stirring $MoCl_4$ and Li_2S in stoichiometric proportions to dry tetrahydrofuran (THF). A black precipitate separates out, and the LiCl formed is removed by repeated washing with tetrahydrofuran and ethyl acetate. The MoS_2 formed was then dried of excess solvent by heating in vacuo at 150°C for 5 h; this product loses <5 wt.% on heating to 500°C, and this weight loss is possibly associated with a little excess sulfur. Amorphous MoS_2 prepared in this manner gives an X-ray diffraction pattern with no recognizable Bragg reflections (*Figure 23*). Other dichalcogenides prepared in a similar manner give similar diffraction patterns. Although full structural analysis of these amorphous dichalcogenides are currently unavailable, preliminary evidence indicates that the layered structure is retained at some level. Pressing the amorphous solid in a laboratory press at approximately 100 atm causes the appearance of a low angle reflection at 2θ smaller than the crystalline 002 reflection (*Figure 24*). This may indicate the beginning of ordering due to the lining up of randomly folded layers. If this were true, the amorphous dichalcogenides would be the first member in the series previously described for poorly crystalline 'rag' MoS_2. However, complete analysis of the diffraction patterns is required before this conclusion can be supported. Further evidence for retention of the layered structure comes from infrared (IR) spectra shown for some of the amorphous layered chalcogenides in *Figure 25*. IR spectra of pure samples show no feature other than the M-S vibrations. Crystalline and amorphous TiS_2 showed broad bands with the crystalline band appearing at 405 cm^{-1} and the amorphous band at about 365 cm^{-1}. The reason for this shift is not now understood. VS_2 showed a shoulder at approximately 400 cm^{-1}. The MoS_2 peak for amorphous MoS_2 was broad and occurred at 365 cm^{-1} which is the same place at which the crystalline MoS_2 peak occurs. However, the width of this peak in MoS_2 is affected by crystallinity. The infrared properties of these materials will be the subject of a future report. In general there is an increasing tendency to stabilize lower crystallinity as one proceeds from group 4B to group 7B. Thus, MoS_2 is completely amorphous as prepared at room temperature and

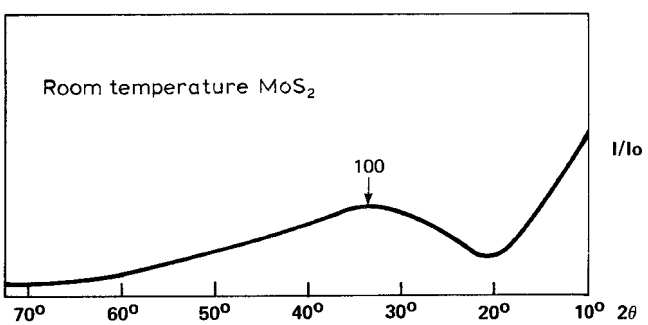

FIG. 23. X-ray pattern of amorphous MoS_2 (100 indicates position of Bragg peak in crystalline MoS_2).

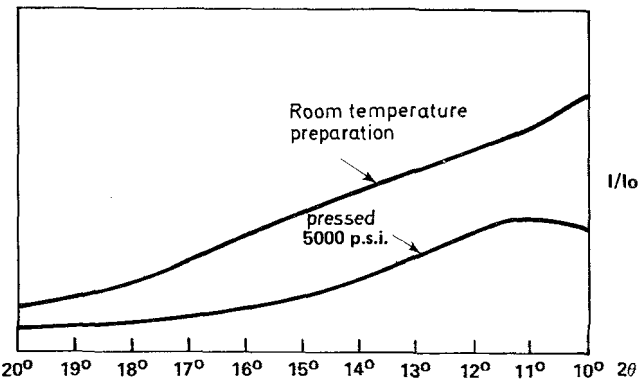

FIG. 24. Effect of pressure on the low angle scattering of amorphous MoS_2.

poorly crystalline when treated at 400°C in H_2/H_2S. TiS_2 and VS_2 show indications of Bragg peaks at room temperature and will crystallize at 400°C. On the other hand amorphous ReS_2 can be prepared which is stable at 400°C.

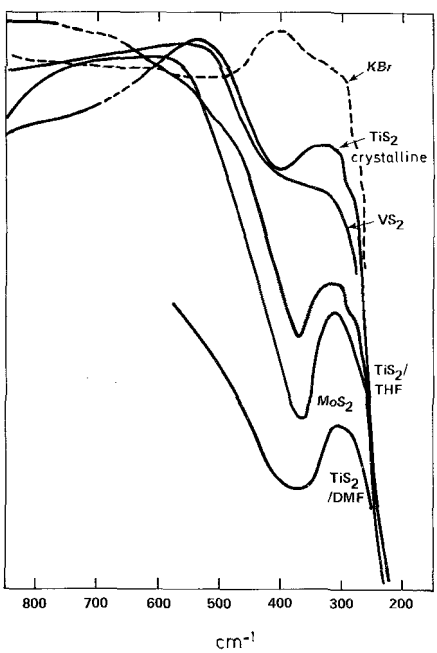

FIG. 25. IR spectra of amorphous dichalcogenides (from Chianelli *et al.*, 1979a).

Osmium disulfide OsS_2

OsS_2 represents an interesting example of a dichalcogenide which exists in three different forms: amorphous, poorly crystalline with a layered structure and crystalline with the pyrite structure. A specific example of how a transition metal chalcogenide can

be prepared by low temperature precipitation is provided by OsS_2. $OsCl_4$ (4 g) was added to 100 ml of ethyl acetate yielding a greenish solution. To this was added 1.12 g of anhydrous Li_2S which caused the solution to turn black with stirring. The solution was filtered, washed with ethyl acetate and air dried yielding a black powder (amorphous OsS_2) which was treated at 400°C in a stream of $H_2/15\%/H_2S$. The resulting black powder weighed 2.80 g (theoretical $OsS_2 = 3.10$ g) with a BET surface area of 20 m^2/g. Further analysis discussed below indicated that the OsS_2 produced was a previously unknown layered compound which could be converted to the known pyrite structure by heating in vacuum or $H_2/15\%/H_2S$ above 600°C. OsS_2 can also be prepared by thermal decomposition of the ammonium hexachloride in H_2S:

$$(NH_4)_2OsCl_6 + 2H_2S \xrightarrow[3\,h]{220°C} OsS_2 + 2NH_4Cl(s) + 4HCl(g) \qquad (8)$$

$(NH_4)_2OsCl_6$ was heated in a stream of H_2S at 220°C for 3 h. The product was extracted with methanol for 24 h in a Soxhlet extractor to remove residual (NH_4Cl). This was followed by a CS_2 extraction for 12 h to remove excess sulfur.

The product at this point gave a completely amorphous powder diffraction pattern. Thermogravimetric analysis of the product showed that the Os:S ratio was 1:2.07 indicating that the amorphous disulfide was obtained (Passeratti *et al.*, 1979). Heating amorphous OsS_2 in vacuum from room temperature to 900°C causes dissociation of the solid and Os metal to be left behind. However, heating to 800°C in a sealed quartz tube for four days causes the amorphous OsS_2 to crystallize to the known pyrite phase. Heating the amorphous OsS_2 in a stream of H_2S at 450°C for 2 h caused the crystallization of OsS_2 in the layered structure. The transition from the amorphous to the poorly crystalline layered phase can be seen in the X-ray diffraction patterns shown in *Figure 26*.

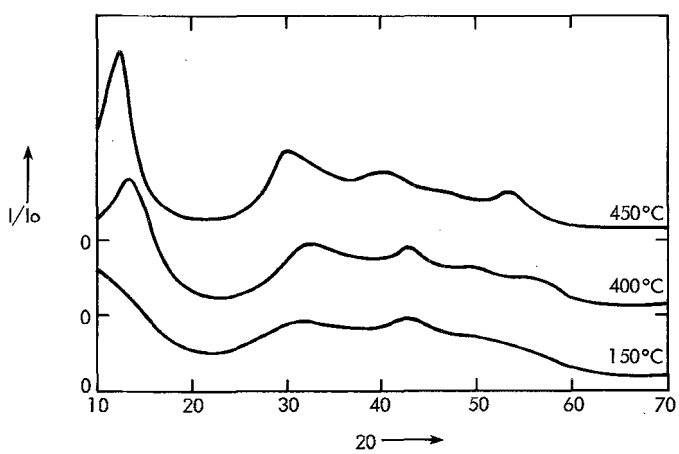

FIG. 26. X-ray scattering for OsS_2 at various temperatures of pretreatment.

A transmission electron micrograph of amorphous OsS_2 prepared by thermal decomposition is shown in *Figure 27*. We may note the porosity and connectivity of the structure. It almost appears as if the compound melted during formation. The pores which are in the 100–500 Å region were probably formed by gases which must escape from the solid precursor during thermal decomposition in H_2S. It is remarkable that the morphology shown in *Figure 27* persists with little change as one goes from the

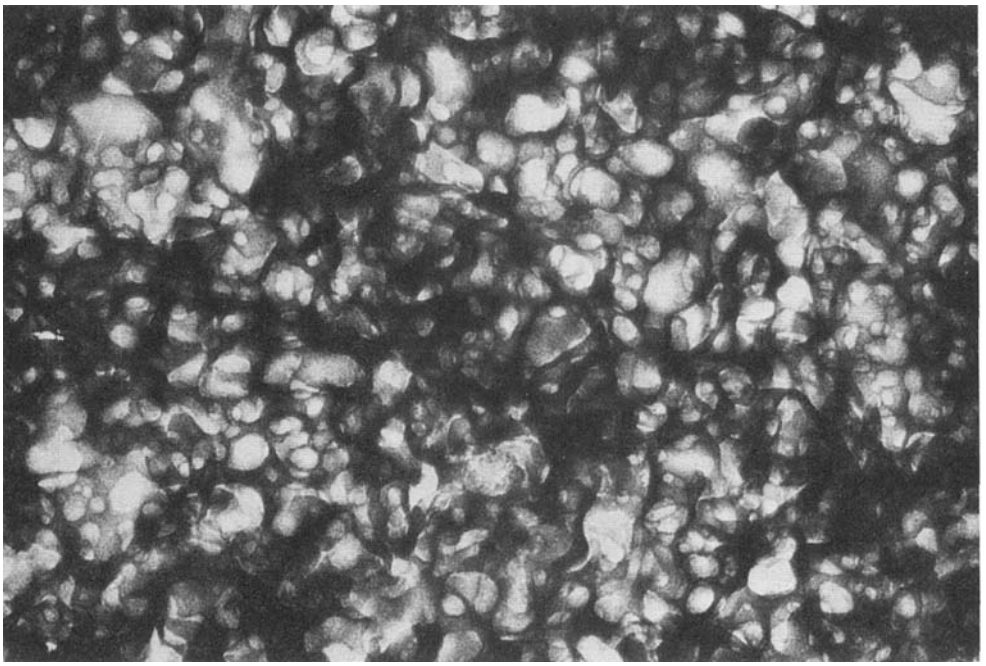

FIG. 27. TEM of amorphous OsS_2 (× 180 000).

amorphous state to the poorly crystalline state and then to the crystalline state. Although the structure of amorphous OsS_2 is presently unknown we believe that it is related to that of the layered form of OsS_2 based upon infrared evidence of the type previously described for amorphous MoS_2. The fact that OsS_2 can exist in both the layered dichalcogenide structure and the pyrite structure is quite interesting. Based upon the poorly crystalline X-ray pattern of layered OsS_2 (*Figure 14*) we assume octahedral coordination. OsS_2 in the pyrite structure also has octahedral coordination and the structure looking down the 111 axis is very similar to the layered dichalcogenide structure. The major difference being the formation of the sulfur–sulfur linkages which give rise to the three dimensionality of the pyrite structure. The transformation of layered OsS_2 to pyritic OsS_2 can be viewed as an internal redox:

$$\begin{aligned} Os^{IV} + 2e^- &\rightarrow Os^{II} \\ 2S^{=} &\rightarrow S_2^{=} + 2e^- \end{aligned} \tag{9}$$

This is an illustration of the close proximity of the metal d-electrons and the sulfur p-electrons. It is this property which is at the heart of the interesting chemical and physical properties of these materials.

Amorphous MoS_2

Crystalline MoS_2 reacts in electrochemical cells with only about 0.1 Li/Mo (Besenhard *et al.*, 1976). In this case, X-ray diffraction data suggests that this reaction is a result of the formation of lithium sulfide and not of an intercalated MoS_2, and this decomposition is in agreement with thermodynamic predictions (Whittingham and Gamble, 1975). In

contrast (Jacobson *et al.*, 1979b), when a chemical lithiating agent such as n-butyl lithium is used, around 1.5 Li/Mo are consumed (*Table 1*). Amorphous MoS_2 may be converted into crystalline MoS_2 by thermal treatment. Crystallization although initiated on heating at around 200–300°C is not complete until 800°C. A very large increase in the surface area, found on heating the material to 200–300°C, is suggestive of a radical reorganization of the crystalline structure. *Table 3* shows these surface areas, measured by standard BET techniques, and the capacities of the sulfides in lithium cells to a 1.4 volt cut-off at 0.5 ma/cm^2 ($LiClO_4$/dioxolane electrolyte). Very clearly the low temperature MoS_2 structure has a substantially larger capacity for electrochemical reaction with lithium than the common crystalline MoS_2 (>800°C sample). The discharge behavior is shown in *Figure 28*. Whereas the two lowest temperature samples show a smoothly varying voltage/composition profile, the break in the curve of the 400°C sample is suggestive of the presence of two phases. At higher temperatures, the capacity falls off rapidly just as reported earlier for crystalline MoS_2 (Besenhard *et al.*, 1976; Whittingham and Gamble, 1975).

TABLE 3. Properties of MoS_2

Temperature (°C)	*Surface area* (m^2/g)	*Capacity* (Li/Mo)
150	5	0.83
275	50	1.12
400	63	0.37
600	44	0.11
Crystalline	<5	0.03

Equally surprising, it was found that this low temperature molybdenum sulfide phase is highly reversible; even after 244 discharge/charge cycles the electrochemical capacity exceeded 50% of that of the second discharge. This data is shown in *Figure 29*. The 400°C sample also showed high reversibility, but at a much lower capacity, ~0.2 Li/Mo on the second discharge dropping to ~0.1 after 500 cycles.

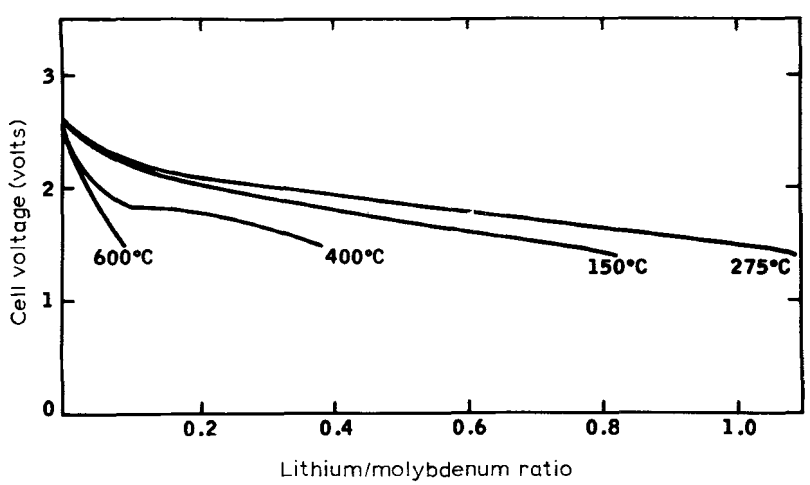

FIG. 28. Effect of heat treatment on MoS_2 in lithium cells (from Jacobson *et al.*, 1979).

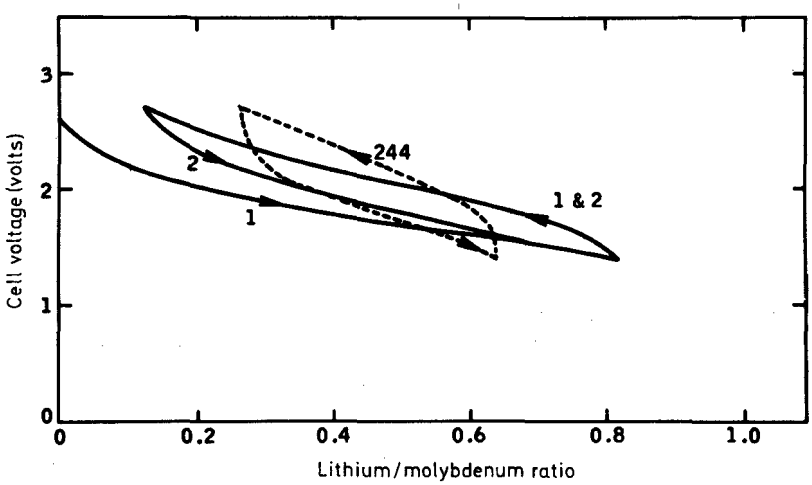

FIG. 29. Cycling behavior of 150°C dried MoS_2 in lithium cells (from Jacobson *et al.*, 1979b).

The sloping discharge/charge data on *Figure 29* bears a similarity to that of the Li/TiS_2 reaction, which may suggest that a similar non-stoichiometric reaction may also be taking place between lithium and this amorphous molybdenum sulfide phase. If high x-value phases of the formula Li_xMoS_2 are formed then the amorphous MoS_2 phase is at least kinetically more stable than the crystalline phase, with respect to the reaction.

$$MoS_2 + Li_xMoS_2 \rightarrow Li_2S + Mo \quad (x > 0.1) \tag{10}$$

Whether this apparent stability reflects a difference in the electronic (i.e. long range) structure or in the local bonding environment is unknown. We may speculate that if the coordination about the Mo in amorphous MoS_2 was octahedral rather than trigonal prismatic there would be room in the conduction band to place more electrons and thus facilitate the reversible reaction with lithium. Nevertheless, we have in amorphous MoS_2 an example of an amorphous material which is superior to its crystalline analog in at least one useful property.

AMORPHOUS CHALCOGENIDES WHICH HAVE NO CRYSTALLINE ANALOGS

A class of amorphous chalcogenides exist which have no direct crystalline counterparts. These include compounds such as MoS_3, $MoSe_3$, WS_3, WSe_3 (the trichalcogenides) V_2S_5, and Re_2S_7. They are generally made by thermal decomposition of the corresponding ammonium thiosalts (Diemann and Müller, 1973):

$$(NH_4)_2MoS_4 \xrightarrow{250°C} MoS_3 + H_2S\uparrow + 2NH_3\uparrow \tag{11}$$

$$2(NH_4)_3VS_4 \xrightarrow{250°C} V_2S_5 + 3H_2S\uparrow + 6NH_3\uparrow \tag{12}$$

These decompositions are usually followed thermally as indicated in *Figure 30*. The structures of these amorphous materials were first studied by Diemann and co-workers (Diemann, 1977a and b; Diemann and Müller, 1978). The compounds V_2S_5 and Re_2S_7 appear to have disordered structures closely related to the usual CdI_2 structure found in the crystalline dichalcogenides. In the case of V_2S_5 based upon combined evidence from vibrational spectra, small angle and wide angle X-ray scattering, photoelectron spectroscopy and thermogravimetry, the authors concluded that each vanadium atom is surrounded by six sulfur atoms at an average distance of 2.34 Å and six vanadium atoms at a distance 3.42 Å. The short range order corresponds to a strongly disordered layered structure. Packing considerations and thermogravimetric evidence are invoked making the layered structure likely. The authors choose a microcrystallite model with 20–25 Å microcrystallites to explain the structure and stoichiometric properties of the compound. It should be considered that if these compounds retain their highly anisotropic structures in the amorphous state they would be very unlike most amorphous materials which are more three dimensional in nature. Thus, the search for direct proof of retention of layers in these amorphous compounds remains one of the most important goals of future work.

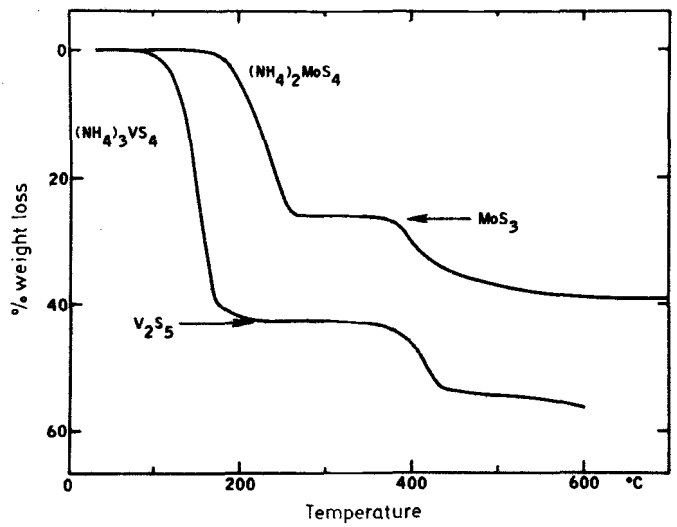

FIG. 30. Thermal decomposition preparations of amorphous chalcogenides.

Amorphous V_2S_5 turns out to be a reversible Li battery cathode like amorphous MoS_2 (Jacobson and Rick, 1980). The compound reacts with six lithium atoms or three lithium per vanadium:

$$V_2S_5 + 6Li \rightarrow Li_6V_2S_5 \tag{13}$$

The cycling data obtained for V_2S_5 in lithium cells is shown in *Figure 31*. The discharge data are seen to be smoothly varying over the whole composition range and there is a definite though broad end point at the end of the discharge. As *Figure 31* shows there is a marked reduction in capacity on the second discharge cycle. The capacity continues to decrease with repeated cycling but eventually levels out to about one third of the initial capacity, ~0.8 Li/V. The fall in capacity is accompanied by a noticeable increase in the voltage profile suggesting that the cathode material is

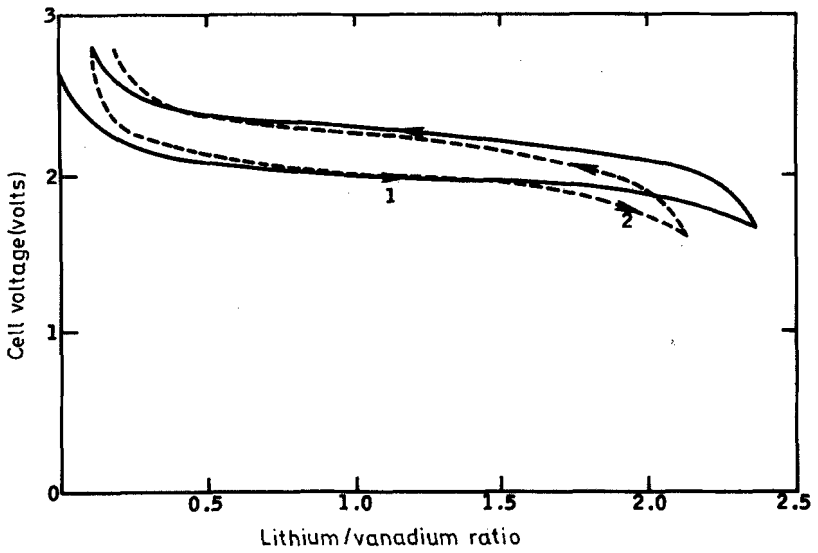

FIG. 31. Cycle behavior of V_2S_5 in lithium cells.

changing in composition; the mean discharge voltage is 1.96, 2.05, 2.12, and 2.28 volts on cycles 1, 2, 12 and 30. The discharge/charge curve separation also changes, markedly decreasing—340, 250, 130, and 100 mV on the above cycles; this again is suggestive of cathode material changes. This phase could conceivably be an amorphous form of VS_2, but there is no definitive structural evidence available yet. However, as pointed out in a previous section amorphous VS_2 picks up about 1.5 lithium per vanadium thus the decrease in capacity would be consistent with the decomposition of V_2S_5 to VS_2.

MoS_3 on the other hand cycles very well for three lithium atoms as indicated in *Figure 32*. Its behavior in this respect is very similar to $NbSe_3$ (Jacobson *et al.*, 1979a).

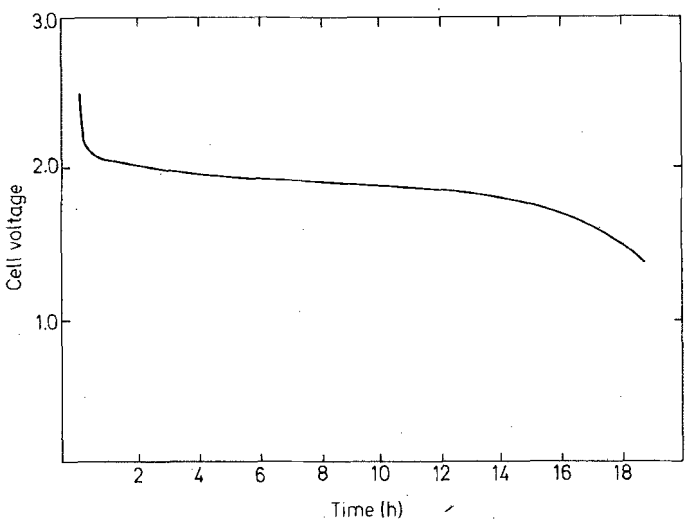

FIG. 32. Discharge curve for MoS_3.

The amorphous trichalcogenides

The structure of amorphous trichalcogenides of Mo and W of Group VIB have been the subject of several studies (Diemann, 1977b; Voorhoeve and Wolters, 1970; Ratnasamy *et al.*, 1973; Stevens and Edmonds, 1975; Liang *et al.*, 1980a and b). The earliest results of these studies suggested that amorphous (a-) MoS_3 was not an independent compound but a mixture of MoS_2 and non-crystalline sulfur. Later, from analysis of the X-ray radial distribution functions (RDF), Diemann concluded that these amorphous trichalcogenides were genuine compounds, although ambiguities remained concerning their detailed structure. The most recent structural studies on a a-MoS_3 and a-WS_3 using high resolution RDF and XPS (X-ray photoelectron spectroscopy) revealed the unique structural features of these compounds. A chain-like structure similar to that of the crystalline trichalcogenides of the neighboring IVB and VB elements was proposed. Along the chain, adjacent metal atoms are bridged with three S atoms. The results also showed dimerization of the metal atoms along the chain and the presence of polysulfide bonds. A formal charge state, $M^{V}(S_2^{=})_{1/2}\ S_2^{=}$, for these amorphous trichalcogenides was therefore proposed.

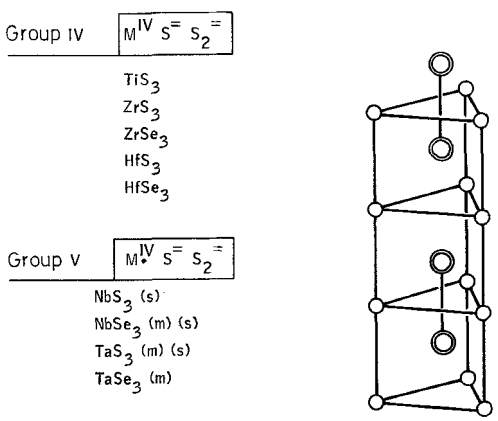

FIG. 33. Structure of NbS_3 O = Se and ◎ = Nb.

The evidence for the above structure will be discussed below. But the chemical analogy to the crystalline trichalcogenides for MoS_3 is rather convincing. The group IV and group V trichalcogenides have the linear chain structures as indicated in *Figure 33* for NbS_3 (Rijnsdorp and Jellinek, 1978). The group IV trichalcogenides are all insulators or semiconductors with the formal valence structure ($M^{IV}S^{=}S^{=}$). The group V trichalcogenides have one more electron on the metal, and thus the metal can pair as indicated in *Figure 33* or some fraction of electron per metal can go into the conduction band. Because of this the group V trichalcogenides can undergo metal-insulator transitions which are of considerable interest because of the so-called 'charge density waves' occurring in these compounds (Fleming *et al.*, 1978; Samborigi *et al.*, 1977). In the group IV trichalcogenides the chains are paired with the nearest neighbor chain translated one-half a unit cell along the chain axis (*Figure 34*). This causes the metal atom to be eight coordinate rather than six coordinate when one considers the next nearest metal atoms in adjacent chains which occur from 2.6–2.8 Å away. Another characteristic of these compounds is the van der Waals gap of dichalcogenide bonds which terminate the layers of double chains in the group IV transition metal trichalcogenides (*Figure 34*). Thus, the compounds have primarily a

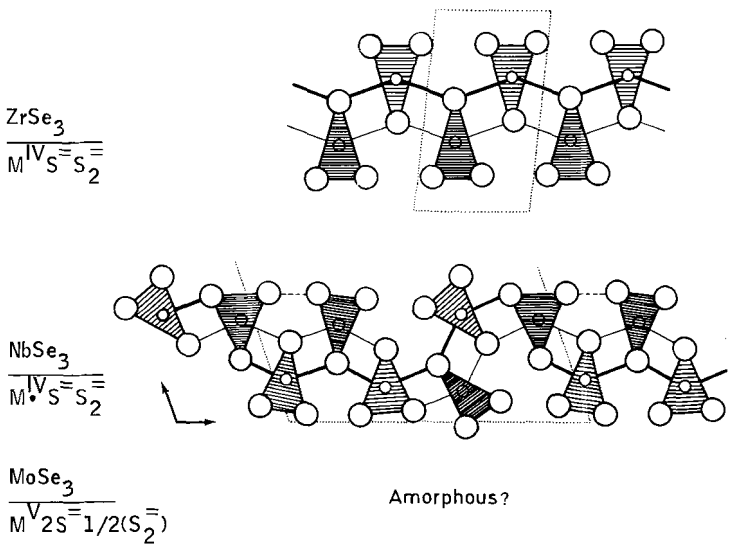

FIG. 34. Chain character of sulfur sub-lattice in the MS_3 structure.

FIG. 35. Crystal of lithiated HFS_3.

chain structure but also a layered character (the chain-like nature can be seen in *Figure 35*). In group V this layered character becomes stronger because of stronger interaction between chains. In $NbSe_3$ there are six distinct chains in the unit cell and some chalcogen–chalcogen distances (indicated by dashed lines in *Figure 34*) between chains are within bonding distances. Some unit cells in group V are even more complicated, especially for the selenides. Thus, there appears to be a tendency toward 'disorder' on the chalcogen lattice as we go from group IV to V and from sulfur to selenium. One reason for this may be that as we go to the right in the periodic table the electronegativity of the metal and the chalcogens become closer. Thus, niobium can 'choose' between two closely lying states:

$$\begin{aligned}&(Nb^{IV}\cdot\cdot Nb^{IV})\tfrac{1}{2}Se^{=}(Se^{-}\cdot\cdot Se^{-})\\ \text{or}\quad &Nb^{V}2Se^{=}(Se^{-}\cdot\cdot Se^{-})\tfrac{1}{2}\end{aligned} \tag{14}$$

In molybdenum with an even closer electronegativity to the chalcogen and with three common valance states

$$(Mo^{IV}\text{: }Mo^{V}, Mo^{VI}) \tag{15}$$

available there are three states to choose from:

$$\begin{aligned}&Mo^{IV}\text{: }Se^{=}(Se^{-}\cdot\cdot Se^{-})\\ \text{or}\quad &(Mo^{V}\cdot\cdot Mo^{V})2Se^{=}(Se^{-}\cdot\cdot Se^{-})\tfrac{1}{2}\\ \text{or}\quad &Mo^{VI}\,3Se^{=}\end{aligned} \tag{16}$$

Thus, the chalcogen–chalcogen bonding system may become delocalized over the chalcogen lattice causing the chalcogen lattice to become disordered. This may be the reason why $MoSe_3$ is amorphous and attempts to crystallize it have so far failed. However, we can say that this feature of 'valance options' is one of the most interesting features of these compounds and is probably at the origin of their interesting and useful properties.

The structure of the amorphous trichalcogenides

What is the evidence for the structure of these compounds? The evidence for the chain structure is based upon EXAFS, X-ray radial distribution analysis, XPS, magnetic susceptibility and vibrational spectroscopies (Liang *et al.*, 1980a and b). The local atomic arrangements of a-MoS_3 and a-WS_3 were studied using X-ray RDF and EXAFS. The radial distribution function of a-WS_3 obtained from the X-ray diffraction measurements using MoKα radiation is shown in *Figure 36*. For the following

TABLE 4. Coordination numbers for the proposed structure of a-WS_3

Partial RDF	*2.64 Å*	*2.83 Å*	*3.24 Å*
$\rho\underline{W}$-W	0	1	1
$\rho\underline{W}$-S	6	2	0
$\rho\underline{S}$-W	2	2/3	0
Cal. area	3552	2580	1369
Exp. area	3261	2029	1237
% Difference	−8.2%	−21.3%	−9.6%

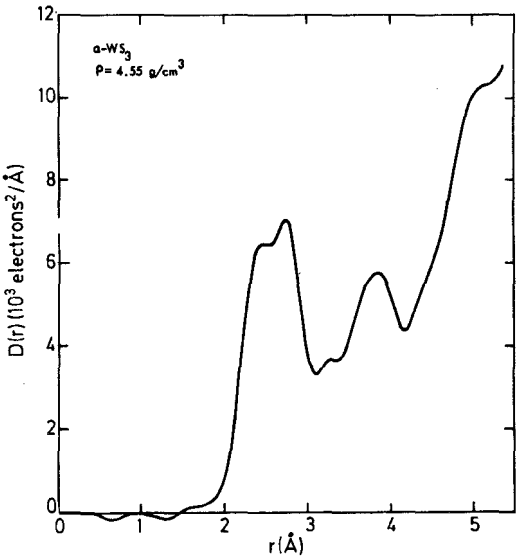

FIG. 36. Radial distribution function for WS_3.

discussion, we are particularly interested in the first three peaks of the RDF which are closely related to the EXAFS results. Using curve fitting with Gaussian peaks, the positions, widths and areas of these peaks are obtained (*Table 4*). The presence of a strong peak at 2.8 Å and only a weak peak at 3.2 Å indicates that a-WS_3 is not a mixture of WS_2 and S. The proposed structure is shown in *Figure 37*.

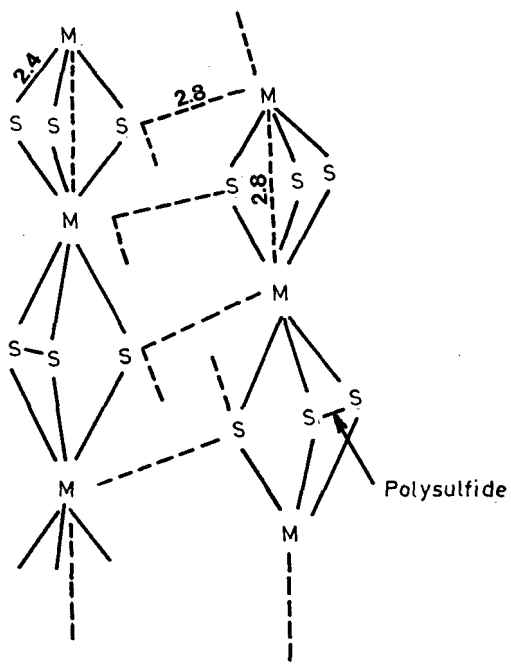

FIG. 37. Proposed structure for WS_3 and MoS_3.

Based on a given structure, the theoretical values of the areas of RDF peaks can be calculated from the relation,

$$\rho_{ab}(d) = X_a N_{ab}(d) Z_a Z_b \tag{17}$$

where $\rho_{ab}(d)$ is the calculated area due to type a atoms coordinated by N_{ab} type b atoms at a distance d, X_a is the atomic percent of type a atoms, Z_a is the electron density of a type a atom which can be approximated by the atomic number. The calculated values of different atomic pairs are given separately in *Table 4* so that comparisons with the EXAFS results can be easily made later. The S–S pairs are not included because of their small contribution to the RDF areas due to the low Z value of S in comparison with W.

The proposed structure of a-MoS_3 and a-WS_3 is the chain-like structure similar to that of the crystalline trichalcogenides of the neighboring groups IVB (Ti, Zr, Hf) and VB (Nb, Ta). Along the chains, there are alternate short (2.8 Å) and long (3.2 Å) metal–metal distances corresponding to the ρW–W values shown on *Table 4*. Each metal–metal pair is bridged with three S atoms with a metal–sulfur distance of 2.4 Å. The metal–sulfur distance at 2.4 Å and metal–metal distance at 3.2 Å are close to the corresponding interatomic distances in crystalline WS_2. However, the short W–W distance of 2.8 Å reveals the formation of metal–metal bonds due to strong metal–metal interaction.

In order to account for the strong RDF peak at 2.8 Å, the proposed structure also includes inter-chain correlations at this distance (ρW–S and ρS–W at 2.8 Å in *Table 4* and *Figure 37*). Each W would be coordinated with 2S and one third of the S with 2W in the adjacent chains to form a super layered structure.

The agreement between the experimental values and the calculated areas of RDF peaks of a-WS_3 based on the above proposed model is reasonably good. The calculated values are larger than the experimental values by ~10% for the 2.4 Å and 3.2 Å peaks. This may partly be due to a density deficiency arising from the porous nature of the thermally decomposed samples. Very intense X-ray scattering at low angles was recently observed on these amorphous samples. Since the small-angle scattering has not been included in our RDF analysis, its effect on the RDF peak area has to be studied. The larger discrepancy shown on the 2.8 Å peak could be due to the disorder of the inter-chain correlation, since the calculation is based on an ordered structure.

Due to the fluorescence problem using MoKα radiation, the RDF for a-MoS_3 was obtained only using CuKα radiation. A broad peak corresponding to the sum of the 2.4 Å and 2.8 Å peaks in the a-WS_3 case was observed at 2.45 Å with a peak area of 2953 electrons (using a density value of 3.04 g/cm^3). This value is quite close to the calculated value of 3129 electrons based on the above proposed structure.

The principle of EXAFS and its application to the study of the local atomic arrangement of amorphous materials have been extensively discussed in the literature (Hunter *et al.*, 1977). EXAFS can yield accurate interatomic distances (<0.02 Å). If the amplitude functions and the Debye–Waller factors are known, the coordination numbers and mean relative displacements may also be obtained.

For a-MoS_3 and a-WS_3, EXAFS data using Mo K edge (~20 000 eV) and W L_{III} edge (~10 205 eV) were obtained at Stanford Synchrotron Radiation Laboratory. *Figure 38* shows the Fourier transform of the Mo K edge EXAFS of a-MoS_3. The three peaks assigned on the figure were determined through a curve fitting procedure. It should be noted that the positions and origins of these peaks agree with the results of our X-ray RDF analysis. The curve fitting procedure is described in Liang *et al.*, 1980b. The results of the fit based on a three-shell model are summarized in *Table 5* for a-MoS_3 and a-WS_3, respectively.

TABLE 5. EXAFS fitting parameters

	(M–S)		(M–M$^{(1)}$)		(M–M$^{(2)}$)	
Sample	*N*	$\Delta\sigma^2$	*N*	$\Delta\sigma^2$	*N*	$\Delta\sigma^2$
MoS_3	2.414 Å		2.741 Å		3.145 Å	
	5.93	0.0037	0.93	−0.0010	1.63	0.0037
WS_3	2.379 Å		2.757 Å			
	8.11	0.0171	1.30	−0.0030		

The EXAFs results for a-MoS_3 show that the Mo atoms are coordinated with approximately 5.9 S atoms at 2.41 Å, 0.9 Mo atoms at 2.74 Å and 1.6 Mo atoms at 3.15 Å. For a-WS_3, the quality of the curve fit is less satisfactory. This is partly due to the limited k range accessible for curve fitting. The experimental k range is limited by the W L_{II} edge at 11542 eV. An interesting feature of the $\Delta\sigma^2$ values shown in *Table 5* is their negative sign for the M–M shell at 2.74 Å. This sign is consistent with the formation of metal–metal bonds and consequently the reduction of the mean displacements of the metal–metal pairs relative to the crystalline MS_2 standard. Currently, work is continuing to further refine X-ray and EXAFS data and to extend them to the triselenides.

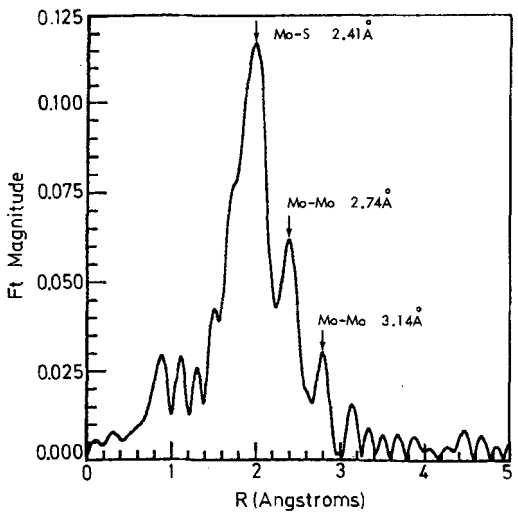

FIG. 38. Fourier transform of MoS_3 EXAFS.

X-ray photoelectron spectroscopy reveals the presence of two types of sulfur species in a-MoS_3, $(S–S)^{=}$ and $S^{=}$ with a 1:2 ratio of their intensities (*Figure 39*). Based on this result, a formal charge state of $M^{V}(S_2^{=})\frac{1}{2}S_2^{=}$ was assigned for these compounds. The spin pairing of M^{V} cations is suggested as the origin of the dimerization of metal atoms in these compounds. Further, the polysulfide species in a-MoS_3 are present in quite a unique ratio. Presumably, one polysulfide is present in every other bridging sulfur triangular. Typical magnetic susceptibility data are shown in *Figure 40*. The data were fitted by the following relation,

$$\chi = \chi_0 + \frac{C}{T-\theta} \tag{18}$$

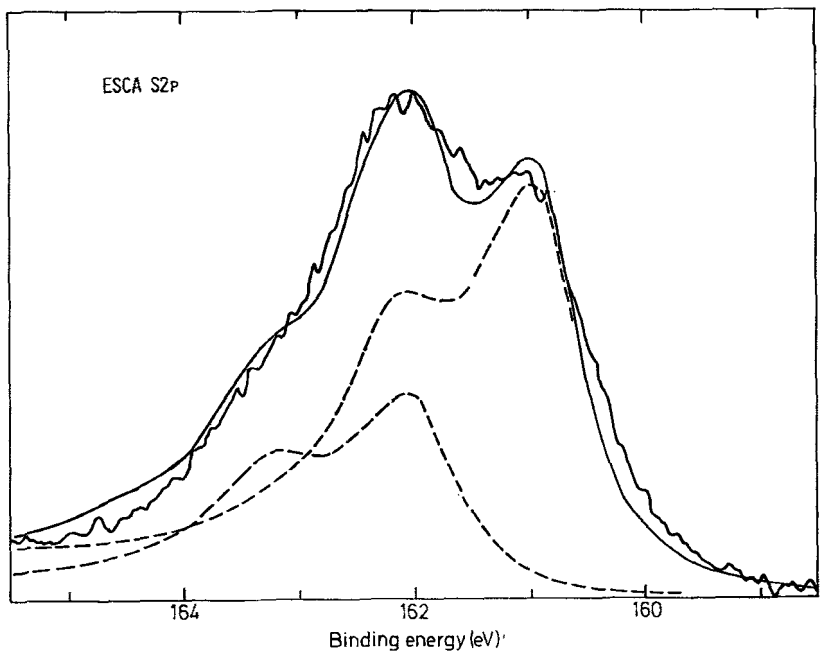

FIG. 39. 2p region of the XPS spectrum of amorphous MoS_3. Dashed lines indicate sulfur 2p spectrum for RuS_2 and MoS_2 respectively. Solid line indicates composite spectrum for $1S^{-}$ and $2S^{=}$ sulfurs.

The temperature independent term χ_0 (-61×10^{-6} cm^3/mole), the Curie constant C (7.0×10^{-3} cm^3-K/mole), and the Weiss temperature θ (≈ -3 K) was determined by a least square fit of the above equation to the data; this fit is shown as a solid line in *Figure 40*. The value of the Curie constant indicates that this sample contained a level of paramagnetic species which is negligible (<2 mole %) compared to the Mo content,

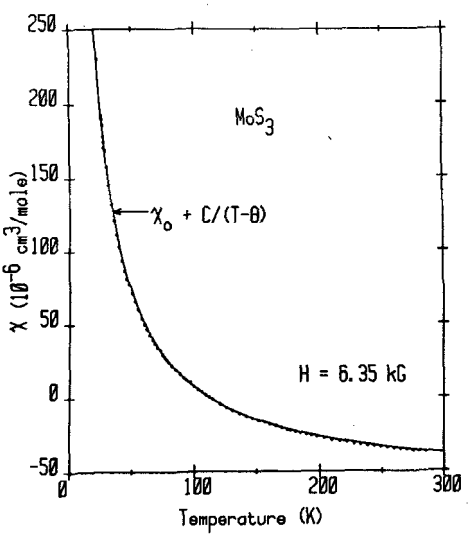

FIG. 40. χ vs. temperature for MoS_3.

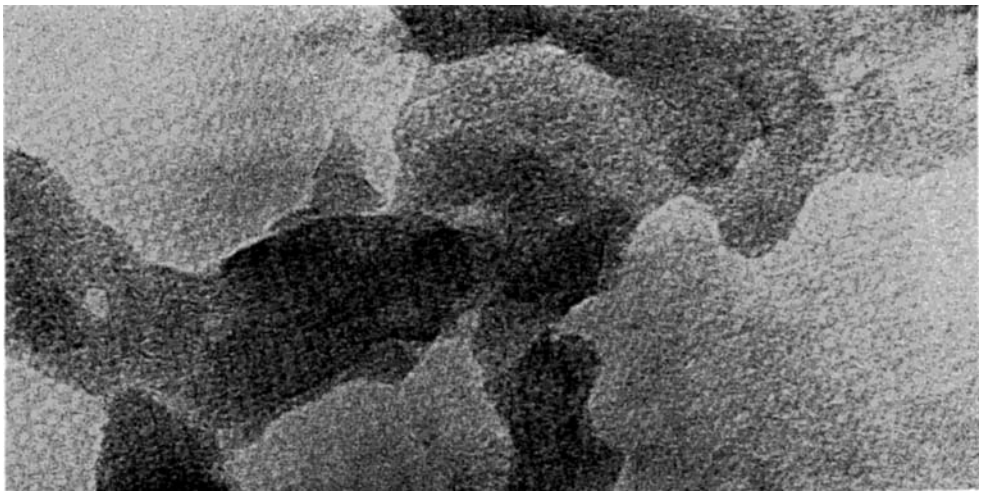

FIG. 41. TEM of MoS_3 (1 mm = 6.8 Å).

and therefore is consistent with our structural and formal charge models for MoS_3 which together require that the Mo^V cations be spin paired to form dimers. Finally, Raman and IR vibrational spectroscopies were also performed to study the local bonding of a-MoS_3. The results are shown in *Figure 41*. These spectra bear no common feature to that of crystalline or amorphous MoS_2. The presence of a broad band at about 520 cm^{-1} in both Raman and IR spectra may be due to polysulfide species.

The above evidence strongly suggests that the local order in the trichalcogenides is consistent with the chain model. There is also evidence for the second chain interaction. But more convincing eivdence for the existence of the chain is needed. We can see from the TEM in *Figure 41* that at this magnification (× 1470000) we see some faint structure appearing. However, more TEM is required to unambigously assign this structure to chains. As stated above the proof of chains in the amorphous trichalcogenides or of layers in the dichalcogenides would add a new dimension of interest to the new class of useful and interesting amorphous solids.

CONCLUSIONS

The amorphous and poorly crystalline transition metal chalcogenides are a class of materials whose wide variation of physical and chemical properties make them a rich area for future investigation. The chemistry of these solids has only been incompletely investigated and it is likely that many new members will be discovered. This is suggested by the rich body of transition metal chalcogenide inorganic chemistry which already exists (Müller *et al.*, 1981). These inorganic molecules can serve as precursors which can be thermally or chemically decomposed to form new amorphous or poorly crystalline solids. Only a handful of the hundreds known have been investigated. In this class of molecules, there are many dimers, trimers, etc., which indicate that we can view these compounds as monomers of polymerized solids containing chains and sheets.

Many of the properties of the amorphous and poorly crystalline chalcogenides are not exhibited by their crystalline counterparts if they exist. We may expect a wide variety of new and useful properties to be discovered. Study of chemistry by these solids

has only just begun. Catalytic and electrochemical studies are described in this report. But many other interesting reactions are to be expected by analogy to their crystalline counterparts. The solid state properties of these compounds are virtually unexplored. Because of the close proximity of the metal d-electrons and the sulfur p-electrons, many interesting solid state effects are to be expected.

Anisotropy plays a large role in the structure of the crystalline and poorly crystalline materials. Yet, the role of anisotropy in the structure of the amorphous transition metal chalcogenides is not clear and represents a challenge to the techniques applied to classic amorphous solids. New techniques available using synchrotron radiation will add considerably to our understanding of anisotropy in these solids. This understanding may lead to new definitions of disorder in solid materials.

ACKNOWLEDGEMENTS

I would like to thank J. P. deNeufville for a critical reading of this review and for encouragement in pursuing this research. And, to M. A. Chianelli for much help and patience in preparing this paper. I would like to recognize the many valuable contributions of my co-workers: A. J. Jacobson, F. Z. Chien, S. C. Moss, J. D. Passaretti, A. Wold, S. P. Cramer, D. C. Johnston, and C. H. Chang. A special thanks to K. S. Liang, whose fine work on the structure of disordered materials, has made this work possible.

REFERENCES

ALCOCK, N. W. and KJECKSHUS, A. (1965). *Acta. Chem. Scand., 19*, 79.

BESENHARD, J. O., MEYER, H. and SCHOLLHORN, R. W. (1976). *Z. Naturforsch., 316*, 907.

CHIANELLI, R. R. (1976). *J. Crystal Growth, 34*, 239.

CHIANELLI, R. R. and DINES, M. B. (1978). *Inorganic Chem., 17*, 2758.

CHIANELLI, R. R., PRESTRIDGE, E. B., PECORARO, T. A. and DENEUFVILLE, J. P. (1979a). *Science, 203*, 1105.

CHIANELLI, R. R., SCANLON, J. C. and RAO, B. M. L. (1979b). *J. Solid State Chemistry, 29*, 323.

CHIEN, F. Z., MOSS, S. C., LIANG, K. S. and CHIANELLI, R. R. (1981). *Proceedings of the Seventh International Conference on Amorphous and Liquid Semiconductors*, 8 July 1981, Grenoble, France.

DIEMANN, E. (1977a). *Z. Anorg. Allg. Chem., 431*, 273.

DIEMANN, E. (1977b). *Z. Anorg. Allg. Chem., 432*, 127.

DIEMANN, E. and MÜLLER, A. (1973). *Coord. Chem. Rev., 10*, 79.

DIEMANN, E. and MÜLLER, A. (1978). *Z. Anorg. Allg. Chem., 444*, 181.

ERGUN, S. (1968). *Carbon, 3*, 211.

FLEMING, R. M., MONCTON, D. E. and MCWHAN, D. B. (1978). *Phys. Rev., B18*, 5560.

GAMBLE, F. R. (1978). *Annals of New York Academy of Sciences, 313*, 86.

GAMBLE, F. R., DISALVO, F. J., KLEMM, R. A. and GEBALLE, T. H. (1970). *Science, 168*, 568.

GUINIER, A. (1963). *X-ray Diffraction in Crystals, Imperfect Crystals, and Amorphous Bodies*, San Francisco: Freeman.

HUNTER, S. H., BIENENSTOCK, A. I. and HAYES, T. M. (1977). *Structure of Non-Crystalline Materials*, London: Taylor and Francis.

JACOBSON, A. J. and RICH, S. M. (1980). *J. Electrochem. Soc., 127*, 779.

JACOBSON, A. J., CHIANELLI, R. R. and WHITTINGHAM, M. S. J. (1979a). *J. Electrochem. Soc., 126*, 2277.

JACOBSON, A. J., CHIANELLI, R. R., RICH, S. M. and WHITTINGHAM, M. S. (1979b). *Mat. Res. Bull, 14*, 1437.

LIANG, K. S., DENEUFVILLE, J. P., JACOBSON, A. J., CHIANELLI, R. R. and BETTS, F. (1980a). *J. Non-cryst. Sol., 35* and *36*, 1249.

LIANG, K. S., CRAMER, S. P. JOHNSTON, D. C., CHANG, C. H., JACOBSON, A. J., DENEUFVILLE, J. P. and CHIANELLI, R. R. (1980b). *J. Non-cryst. Sol., 42*, 345.

MÜLLER, A., DIEMANN, E., JOSTES, R. and BÖGGE, H. (1981). *Angew. Chem., Int. Ed. Engl., 20*, 934.

MURPHY, D. W., CROS, C., DISALVO, F. J., WASZCZAK, J. V., MAYER, S. F., STEWART, G. R., EARLY, S., ACRIVOS, J. V. and GEBALLE, T. H. (1975). *J. Phys. Chem., 62*, 967.

MURPHY, D. W. and HULL, G. W. (1977). *J. Chem. Phys., 62*, 973.

PASSARETTI, J. D., KANER, R. B., KERSHAW, R. and WOLD, A. (1981). *Inorg. Chem., 20*, 501.

PECORARO, T. A. and CHIANELLI, R. R. (1981). *J. Catalysis, 67*, 430.

RATNASAMY, P., RODRIQUE, L. and LEONARD, A. J. (1973). *J. Phys. Chem., 77*, 3242.

RIJNSDORP, J. and JELLINEK, F. (1978). *J. Solid State Chem., 25*, 325.

SAMBORIGI, T., TSUTSUMI, K., SHIOZAKI, Y., YAMAMOTO, M., YAMAYA, K. and ABE, Y. (1977). *Sol. State Comm., 22*, 279.

SCHOLLHORN, R., SICK, E. and SERF, A. (1975). *Mater. Res. Bull., 10*, 1005.

SERF, A. and SCHOLLHORN, R. (1977). *Inorg. Chem., 16*, 2950.

STEVENS, G. C. and EDMONDS, T. (1975). *J. Cat., 37*, 544.

TAUSTER, S. J., PECORARO, T. A. and CHIANELLI, R. R. (1980). *J. Cat., 63*, 515.

THOMPSON, A. H. (1978). *Phys. Rev. Lett., 40*, 1511.

THOMPSON, A. H., GAMBLE, F. R. and SYMON, C. R. (1975). *Mater. Res. Bull., 10*, 915.

THOMPSON, A. H. and WHITTINGHAM, M. S. (1977). *Mater. Res. Bull., 12*, 741.

TORNQVIST, E., RICHARDSON, J., WILCHINSKY, Z. and LOONEY, R. (1967). *J. Cat., 8*, 189.

VOORHOEVE, R. J. H. and WOLTERS, H. M. B. (1970). *Z. Anorg. Chem., 376*, 1965.

WEISSER, O. and LANDA, S. (1973). *Sulfide Catalysts, Their Properties and Applications*, New York: Pergamon.

WHITTINGHAM, M. S. (1976). *Science, 192*, 1126.

WHITTINGHAM, M. S. (1978). *Progr. Solid State Chem., 12*, 41.

WHITTINGHAM, M. S. and GAMBLE, F. R. (1975). *Mat. Res. Bull., 10*, 363.

WHITTINGHAM, M. S. and CHIANELLI, R. R. (1977). *Reactivity of Solids*, New York: Plenum, p. 89.

WILDERVANCK, J. C. and JELLINEK, J. (1971). *Less-Common Met., 24*, 73.

WILLIAMS, P. M., PARRY, G. S. and SCRUBY, C. B. (1974). *Phil. Mag., 29*, 882.

WILSON, J. A. and YOFFE, A. D. (1969). *Adv. Phys., 18*, 193.

WILSON, J. A., DISALVO, F. J. and MAHAJAN, S. (1969). *Phys. Rev. Lett., 32*, 193.